MODELLING OF THE DEPLOYMENT BEHAVIOUR OF HIGHLY COMPACTED THIN MEMBRANES

Pandula Manura Liyanage

148052K

Thesis submitted in partial fulfilment of the requirements for the Degree of Master of Science

Department of Civil Engineering

University of Moratuwa

Sri Lanka

September, 2015

DECLARATION

"I declare that this is my own work and this thesis does not incorporate without acknowledgement any material previously submitted for a Degree or Diploma in any other University or institute of higher learning and to the best of my knowledge it does not contain any material previously published or written by another person except where the acknowledgement is made in the text.

Also, I hereby grant to University of Moratuwa the non-exclusive right to reproduce and distribute my thesis, in whole or in part in print electronic or other medium. I retain the right to use this content in whole or part in future works (such as articles or books)."

…… Date: ……

P.M. Liyanage

"The above candidate has carried out research for the Master's thesis under my supervision."

…… Date: ……

Dr H.M.Y.C. Mallikarachchi

ABSTRACT

Modelling of the Deployment Behaviour of Highly Compacted Ultra-thin Membranes

Space structures such as solar sails, solar reflectors, and sun shields have very large surface areas. Hence they require deployable methods to be stored and transported out of the earth's atmosphere in limited cargo capacities available in launch vehicles. A deployable structure changes its shape and geometry to a compact state with the use of folding patterns for convenience in packaging and/or transporting. Ground testing of deployable structures using physical models requires a representative environment, i.e. a zero gravity environment, which can consume a lot of time, effort, and cost, giving rise to the requirement of simulations carried out in a virtual environment. This research develops a modelling technique which can be used to simulate the deployment behaviour of membrane type deployable structures using a commercial finite element analysis software. Commonly used spiral folding pattern was used to demonstrate the modelling technique.

Modification for the fold line arrangement of spiral folding pattern to account for effects caused by membrane thickness; modelling the crease behaviour with the use of rotational springs; and robustness of the analysis indicated by energy histories were three main aspects considered when developing the modelling technique.

Spiral folding pattern was modified by finding the arrangement of nodes in the folded state of the model by providing sufficient offset between planes and checking the ability of the structure to deploy into a plane sheet. This modification was proposed for modules with regular polygonal shaped hubs. Proposed modification was verified with the use of a paperboard model which had a square shaped hub of 10 mm × 10 mm, 15 nodes in a single spiral, and a thickness of 0.28 mm.

Crease stiffness of Kapton Polyimide film was determined comparing data available from an experiment carried out at the Space Structures Laboratory of California Institute of Technology and results of finite element models developed to simulate the experiment.

Finally two finite element models were made from the proposed technique and results of these analysis were discussed on importance of incorporating crease behaviour in finite element models, important aspects of their deployment behaviour, and robustness of analysis.

This research has successfully developed an approach to modify the fold line arrangement of the spiral folding pattern with regular polygonal shaped hubs to account for the geometric effects caused by membrane thickness and a robust technique to model the deployment behaviour of membrane type deployable structures. Crease stiffness of Kapton Polyimide films was modelled as a rotational spring, where the resisting moment is considered to be proportional to the opening angle near the crease. Comparing results of two finite element models, with and without crease stiffness, showed that crease behaviour affects the deployment performance of these structures significantly, and hence it is important to be included in simulations.

Key Words: *deployable structure, finite element analysis, spiral folding pattern, membrane thickness, crease stiffness*

DEDICATION

To anyone who's interested in pursuing research on Origami based deployable structures

ACKNOWLEDGEMENT

First and foremost, I would like to thank my supervisor, Dr Chinthaka Mallikarachchi, for introducing this research topic to me, providing guidance, advice, encouragement, and friendship throughout the research.

I am also thankful to my parents and my brother for showing enthusiasm at my work and providing the required support and encouragement during the progression of the research.

I really appreciate the valuable comments and suggestions given by the progress reviews committee of this Master's degree: Prof Priyan Dias and Dr Leslie Ekanayake of Department of Civil Engineering, University of Moratuwa and Mr Yasoja Gunawardena of Oriental Consultants Co. Ltd which helped me in completing this research successfully.

Senate Research Council of University of Moratuwa and National Research Council of Sri Lanka needs to be acknowledged for providing necessary funding and resources required to realize this research.

Special thanks should be extended to the Space Structures Laboratory of California Institute of Technology headed by Prof Sergio Pellegrino, which provided experimental data which was vital for the completion of the research.

I would also like to thank my colleagues at the Engineering faculty of University of Moratuwa for the numerous interesting and helpful discussions held.

I would like to extend my gratitude for the authors of the literature referred, which contributed to a major part of this research.

Last but not least I would like to thank the academic staff of the Civil Engineering department and the post graduate studies division, University of Moratuwa, for giving me the help required to complete this research.

TABLE OF CONTENTS

LIST OF FIGURES

LIST OF TABLES

LIST OF ABBREVIATIONS

Abbreviation	Description
NASA	National Aeronautics and Space Administration
AU	Astronomic Unit
FRP	Fibre-reinforced Polymer
DIC	Digital Image Correlation
FE	Finite Element
IKAROS	Interplanetary Kite-craft Accelerated by Radiation Of the Sun
VLBI	Very Long Baseline Interferometry
HALCA	Highly Advanced Laboratory for Communications and Astronomy
DOF	Degrees of Freedom
CORM	Components of Relative Motion

LIST OF APPENDICES

1 INTRODUCTION

1.1 Background

Space has been a fascination for humans from very early times, where they gazed at stars in the sky and made stories about constellations. With the advancement of science, people have been able to get accurate scientific details about stars and planets, which are many light years away from the earth, and get over the wild beliefs they had on them.

Solar sails, solar reflectors, and sunshields are some of the structures used in space exploration. During their operational stages many of these structures can have surface areas larger than even a soccer field. Figure 1.1 shows an artistic rendering of a four-quadrant solar sail. Solar sails are made of membranes or collections of interconnected membrane portions, which have mirrored surfaces. Solar sails utilizes the radiation energy of the sun to provide propellant free propulsion for spacecrafts, especially for small space probes like CubeSats. This is a sustainable propulsion method which does not require high power launch vehicles or high volume cargo compartments to carry required propellant.

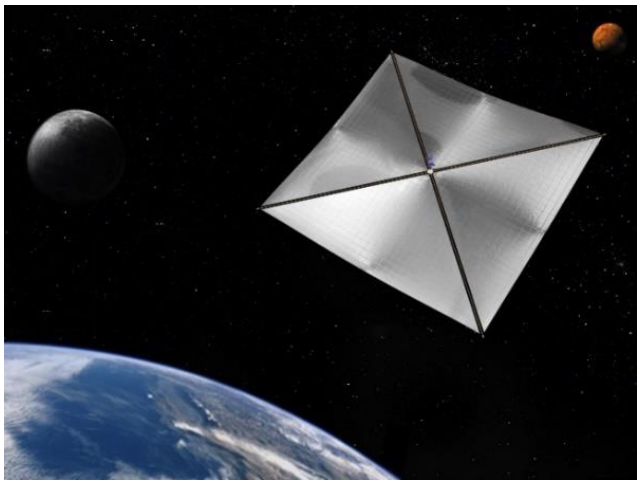

Figure 1.1 – An artist's rendering of a four-quadrant solar sail (Anon, 2011)

In 1865, Jules Verne first brought out the idea of using solar radiation to propel space shuttles, in his novel “From Earth to the Moon”. A yacht race between space ships

propelled by solar sails is mentioned in Arthur C. Clarke's short story "Sunjammer" which was published in 1964. These examples show that the concept of solar sailing is not in any way novel, but still the use of solar sails in space missions are still in infant stages.

Solar sails reflect a small portion of radiation energy from the sun by their mirrored surfaces to gain momentum following the Newton's third law. Availability of miniaturized space probes (e.g., Cubesats) shows great synergy with solar sails in increasing their effectiveness and popularity. Many theoretical and practical work related to astro-dynamics, mission applications, and technology requirements of solar sails has been done in the 21st century (Cubillos & Souza, 2011). Due to the low resistance in space, only a very small force is required to move these structures after it travels out of the earth's atmosphere. Yet, solar sails require very large surface areas to obtain this force.

Generally for a nominal mission of 1 Astronomic Unit (1 AU) from the earth, a solar sail having a reflective area of 10,000 m^2 may be required (Graybeal & Craig, 2006). AU is a distance measuring unit, equal to the mean distance from the centre of the earth to the centre of the sun or 149.6 million km. Figure 1.2 shows a comparison of the size of a solar sail, the Washington Monument, and two space rockets which can carry these structures to space. Saturn V is the largest space rocket available with NASA (National Aeronautics and Space Administration) at present time.

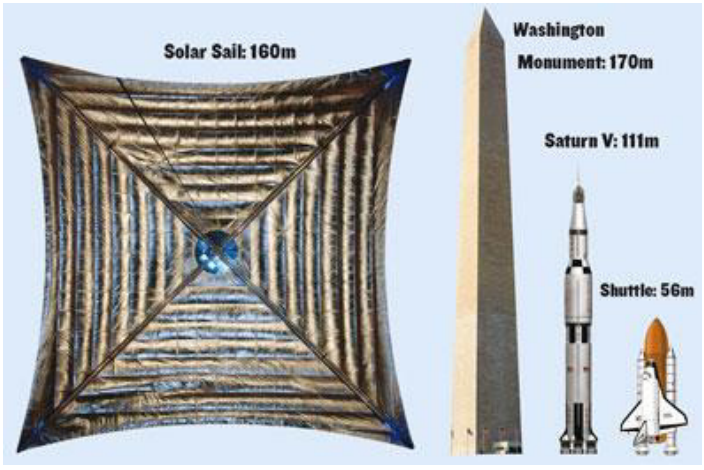

Figure 1.2 – Relative size of NASA's proposed 160 × 160 m solar sail (Anon, 2009)

Large size of these structures require them to adopt deployable, erectable, adaptive, or gossamer structural concepts for storage and transportation purposes, as they need to fit into finite cargo capacities available in launch vehicles (see Figure 1.2). From these, deployable structures is the most widely used concept as a solution to the said limitation. Deployable structures utilize folding patterns based on Origami, the Japanese art of folding paper, to change into a much more compact state for storage and transportation purposes and then deploy back to the original shape once it moves an appropriate distance away from the earth's atmosphere. Material with high strength to weight ratios (gossamer materials) are used to make ultra-thin deployable membranes to improve the efficiency of these structures.

1.2 Deployable Structures

Deployable structure concept is a major structural concept which has been widely used from very early stages of space exploration. A deployable structure can be defined as a structure which changes its shape and geometry to achieve convenience in packaging and transporting.

Simple day-to-day tools such as umbrellas also adopt deployable concepts to achieve ease of packaging and transporting. An umbrella can be folded when it is being carried around and then deploy back to the useful bulky state to give protection from rain.

There are many forms of deployable structures which has very different characteristics from each other. Coiled rods, plates, membranes, structural mechanisms, and retractable domes (Pellegrino, 2001) are some of the deployable structural forms. The scope of this research is limited to deployable structures made from ultra-thin membranes (e.g., solar sails).

1.3 Objectives of the Research

While very complex deployable structures are being built, most of them are developed by trial and error based physical experiments. Due to the large size of these structures, ground testing them in a reduced gravity environment is extremely difficult, time consuming, and expensive. With the rapid development of high performance computers,

researchers now prefer to work in virtual environments (using computer based simulations) to optimize these structures.

For such simulations to be effective, results obtained from analysis should be adequately closer to reality. If not either the safety or the economy of these structures can be adversely affected. In general the thickness of the membrane (Guest, 1994), creases formed in fold lines, and robustness of analysis require special attention in modelling these structures.

Packaging large thin membranes into small volumes inevitably introduces creases, which are regions of high curvature and plasticity. Creases will affect the deployment behaviour of these structures significantly. Thus accurate modelling of creases is critical in deployment simulations.

The main objective of the research was to develop a high fidelity simulation technique to predict deployment behaviour of highly compacted ultra-thin membranes. Developing a simulation technique will reduce the cost, time, and effort spent on testing physical prototypes in an environment representing their operating condition (e.g., zero gravity environment).

To achieve this objective a simulation technique developed required to be robust, incorporates properties of creases, and include a modification to the fold line arrangement to avoid the undesirable stresses caused by thickness of membranes, improving the accuracy of the results given by these simulations.

1.4 Methodology

Main objective of the research was to develop a simulation technique to predict deployment behaviours of highly compacted thin membranes accurately. A brief description of the methodology followed to achieve this objective is given in this section.

An extensive literature review was carried out to find the research that has been carried out in specific areas applicable for the current research. Literature on deployable structures, spiral folding pattern, effects of membrane thickness on folded structures,

approaches available to model the deployment behaviour, and behaviour of creases under loading were reviewed.

Next a method was developed to modify the fold line arrangement of the spiral folding pattern, so that the adverse effects caused by the membrane thickness in the stored configuration are avoided. This modification was verified using physical models made from paperboard.

Properties of creases were determined by comparing data from an experiment carried out at the Space Structures Laboratory of California Institute of Technology, and finite element (FE) models made using the FE analysis software "Simulia Abaqus" to simulate the experiment. A trial and error procedure was followed varying the rotational stiffness of connectors (connectors are used to simulate the stiffness of creases) to obtain the crease stiffness of 25 μm Kapton Polyimide film by matching deformed shapes (crease angle) of the FE model with the physical experiments. All the other properties were kept constant for all models.

Finally FE models for the modified spiral folding pattern were analyzed with and without the crease stiffness. Results from these analysis were critically examined.

1.5 Arrangement of the Report

Following the introduction, second chapter presents the literature review, which was written by conducting a broad, but not a complete review of previous studies carried out on specific aspects relevant for the current research. The first section of this chapter discusses finding on deployable structures in a general manner. In following sections, the review looks at research carried out on: spiral folding pattern, folding mechanisms, effects of thickness of membranes, simulation of deployment behaviour, and behaviour of creases.

Chapter three looks at the adoption, and the validity of the method proposed to modify the spiral folding pattern to account for the effect of membrane thickness.

Obtaining crease properties, and the modelling technique suggested to simulate crease behaviour are discussed in chapter four.

Modelling technique proposed to simulate the deployment behaviour of deployable structures is presented in Chapter five with the use of the spiral folding pattern.

Chapter six presents the discussion and the results of work carried out in current research. Chapter seven completes the report with conclusions and recommendations for future research.

1.6 Outcomes of the research

First, this research has successfully developed an approach to modify the fold line arrangement of the spiral folding pattern with regular polygonal shaped hubs to account for the geometric effects caused by membrane thickness.

Then the crease stiffness of 25 μm thick Kapton Polyimide films was determined where the resisting moment developed at creases showed a linear relationship with the opening angle.

Comparing the results of two finite element models showed that crease behaviour affects the deployment behaviour of these structures significantly, and hence is important to include them in simulations.

Finally a robust technique to model the deployment behaviour of membrane type deployable structures was proposed with the use of the commonly used spiral folding pattern.

2 REVIEW OF PREVIOUS WORK

This chapter concerns research and studies which have preceded the current research and made the background for its development. The first section gives a brief overview on deployable structures, showing examples of their usage in achieving various objectives. This does not provide a complete review on deployable structures, where many other sources have provided findings in various other aspects.

The remaining sections go into specific work that was carried out and relevant for the remaining chapters of the current research. Special emphasis is given to the simulation techniques developed by Liyanage & Mallikarachchi (2013; 2015), which was developed further in the current research.

2.1 Deployable Structures

Even though a majority of applications of the deployable structures concept are space based, some of the simple bits and pieces which comes in handy in day-to-day activities uses the same concept. For example folded road maps, standard envelops as well as umbrellas are commonly seen deployable assemblies.

Deployable methods are used in the field of architecture in structures such as mobile tents, textile screens, antiques arenas, and temporary roofing for sports arenas. Some research have been carried out to check different aspects of these applications. But the fact remains that a majority of the interest which has been directed toward deployable concept is due to its potential applications in space structures.

Space structures such as solar panels, solar sails, antennas, and sunshield are massive structures which can go well beyond the size of a soccer field. But launch vehicles which carries these structures to space have limited storage capacity in their cargo bays. Figure 1.2 compares the size of a solar sail with respect to a normal space shuttle and Saturn V which is the tallest space rocket at 111m. To overcome this mismatch, concepts such as erectable structures, deployable structures, gossamer structures, and adaptive type structures have been proposed and used (Natori, et al., 2010).

Erectable type structures will be taken to space in separate pieces and put together by humans or robots. These types of structures are generally not preferred as sending humans on space missions is not only dangerous but also expensive due to the extra safety precautions that need to be followed. Using robots for such missions is not a viable option as they may not be advance enough to perform some delicate and complex tasks.

Large membranes and light weight booms are used in gossamer type structures to realize large space structures (Sakamoto, et al., 2012). Gossamer type structures aims at making the structure light-weight. This type of structures cannot be used on their own and requires deployable models to realize.

Deployable concept relies on folding patterns for safety and efficiency in packaging and transporting the structures to space and then deploy these structures through various mechanisms (Guest, 1994) such as inflatable tubes, tape springs, etc. In addition this concept saves the structure from loads induced by vibrations taking place during launch. Further this method allows for unmanned missions which will reduce the associated risk and cost. All the above mentioned reasons make the deployable structures concept to be the preferred solution in realising very large structures in space. Deployable structures concept can be applied for many space applications, such as solar sails, satellite antennas, solar panel arrays, sunshields, and solar reflectors.

The 14.0 m × 14.0 m solar sail demonstrator IKAROS (Interplanetary Kite-craft Accelerated by Radiation Of the Sun) (see Figure 2.1), which wrap its light-weight solar sails around a cylindrical body of diameter 1.6 m and height 0.8 m, was successfully deployed on June 2010 (Mori, et al., 2009).

The radio astronomy satellite HALCA (Highly Advanced Laboratory for Communications and Astronomy, see Figure 2.2), which is dedicated for space VLBI (Very Long Baseline Interferometry) observations, which has a 8 m diameter main antenna supported on several mesh type antennas and launched to space in February 1997, followed a deployment process similar to the blossoming of a flower (Kishimoto, et al., 2006).

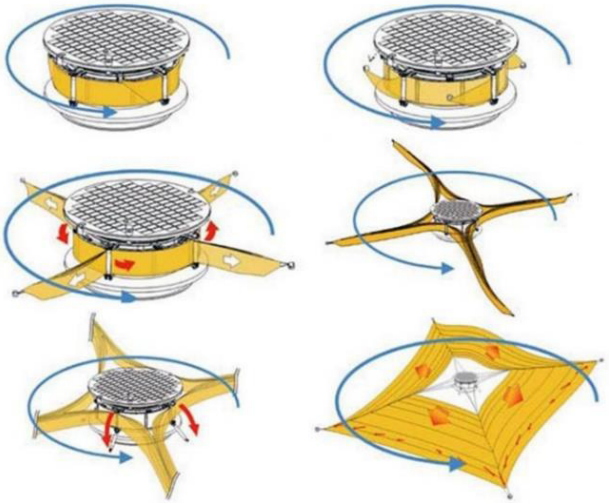

Figure 2.1 - Solar sail demonstrator IKAROS (Warwick, 2010)

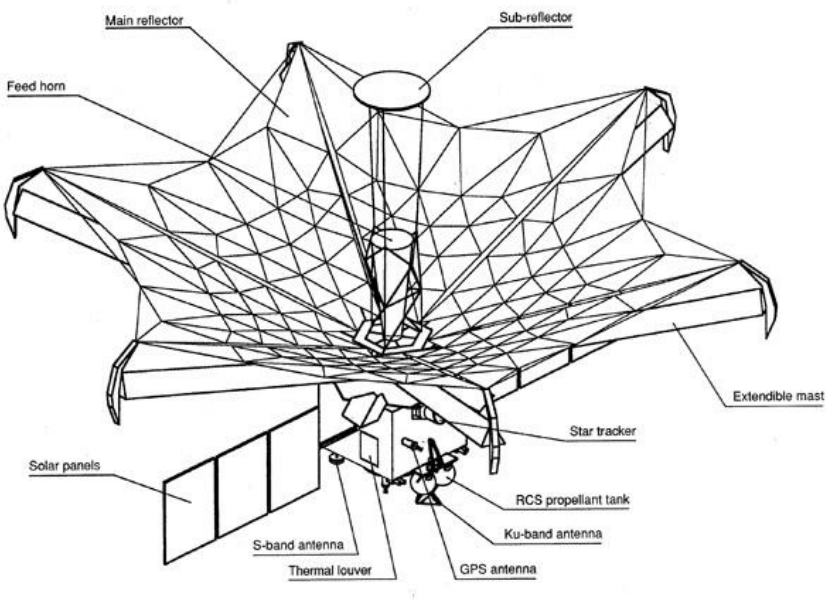

Figure 2.2 - Radio astronomy satellite HALCA – VLBI (Japanese Aerospace Exploration Agency, 2008)

2.2 Spiral Folding Pattern

Spiral folding pattern utilizes a method similar to iso-area twisting to wrap a membrane around a polygonal shaped hub (Lang, 1997). It has well-defined fold lines which prevents undesirable wrinkling between fold lines present in patterns like Origami flasher. Spiral folding pattern can be used for polygonal shaped modules with any number of sides. These polygons do not even have to be regular polygons (generally

the shape of the central hub and the module are kept the same for better deployment performance). Figure 2.3 shows fold line arrangements for modules with regular triangular, square, and regular hexagonal shaped modules which will fold with the spiral folding pattern.

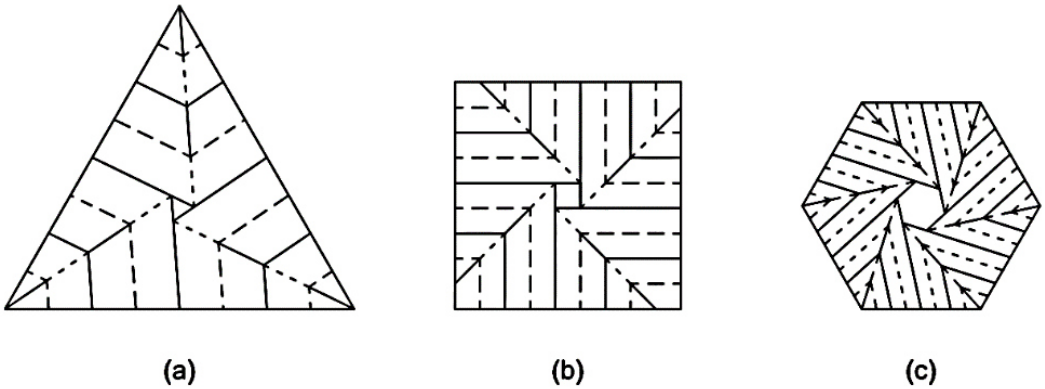

Figure 2.3 - Modules with spiral folding pattern
(a) Triangular shaped module (b) Square shaped module (c) Hexagonal shaped module (Liyanage & Mallikarachchi, 2013)

Snapshots of the deployment of a square shaped module with the simplest arrangement of the spiral folding pattern in which all behaviours of the pattern are represented is shown in Figure 2.4.

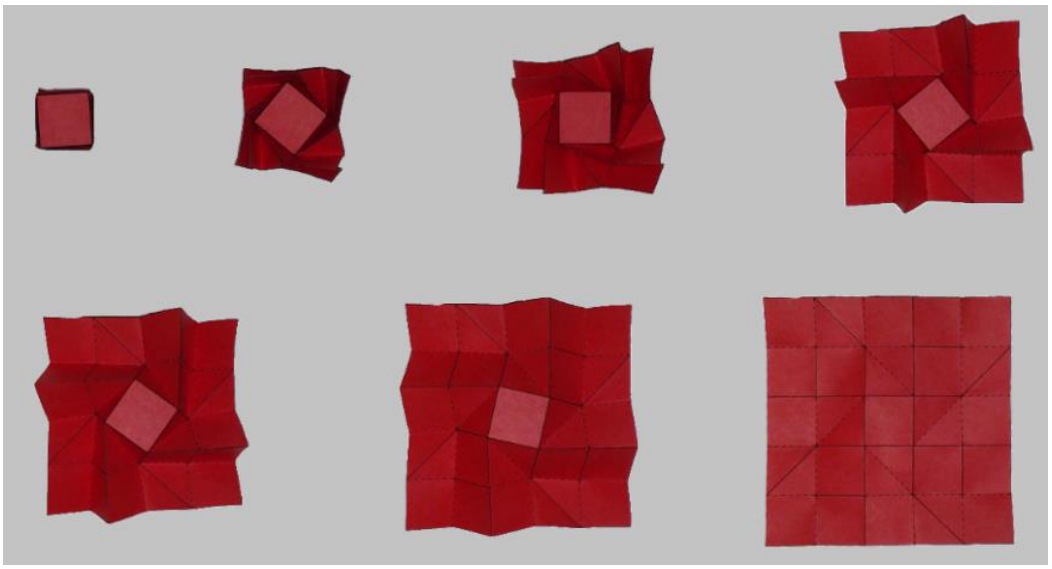

Figure 2.4 - Deployment of a membrane folded with spiral folding pattern

Another positive aspect of the spiral folding pattern is that some modules can be integrated through tessellated patterns, which can be used to break large membranes

into small modules. These modules are not just integrated though their shape, but also from the deployment mechanisms (see Figure 2.5).

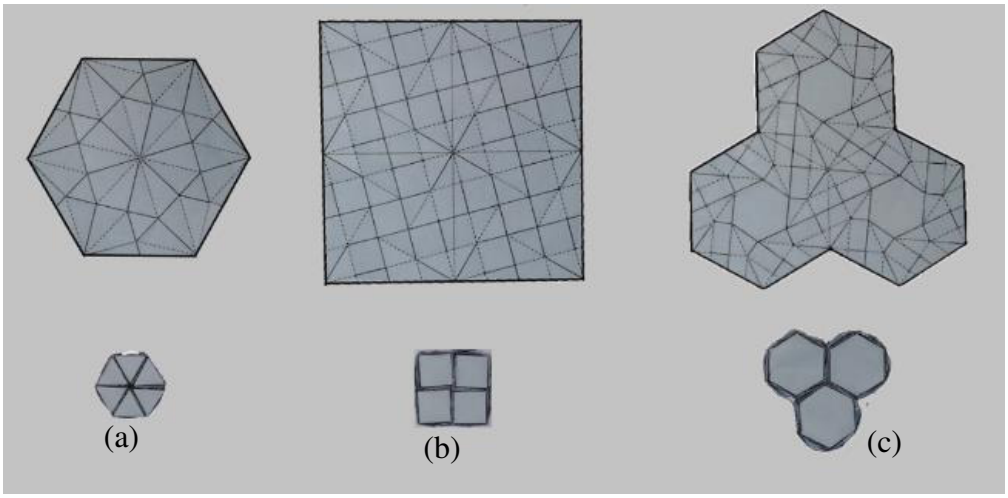

Figure 2.5 - Tessellation of spiral folding modules
(a) Triangular shaped modules (b) Square shaped modules (c) Hexagonal shaped modules

2.3 One-dimensional Folding Mechanisms

Origami is the traditional Japanese art of folding paper, which started in 17th century AD and popularized in the rest of the world in 1900's, is not just a technique which styles articles pleasing to the eye. Origami techniques are used for engineering applications which can be broadly categorized into three main areas: increasing of stiffness in structures with minimal increase in weight, development of shock-absorbing devices, and in realising deployable structures (Schenk & Guest, 2011).

Deployable structures is the most important application of Origami, where the core of the concept is based on folding patterns. This research mainly concerns membrane type deployable structures. However, several research has been carried out on other types of deployable structures: coiled rods, flexible shells, plates, etc. (Pellegrino, 2001; Trautz & Kunstler, 2010).

One dimensional structural elements can be stored in three ways as shown in Figure 2.6: zigzag or Z folding pattern, rollup or circumferential folding, and telescoping folding. Folding patterns of two dimensional structures is developed through combinations of one or more of these folding mechanisms (Sakamoto, et al., 2012).

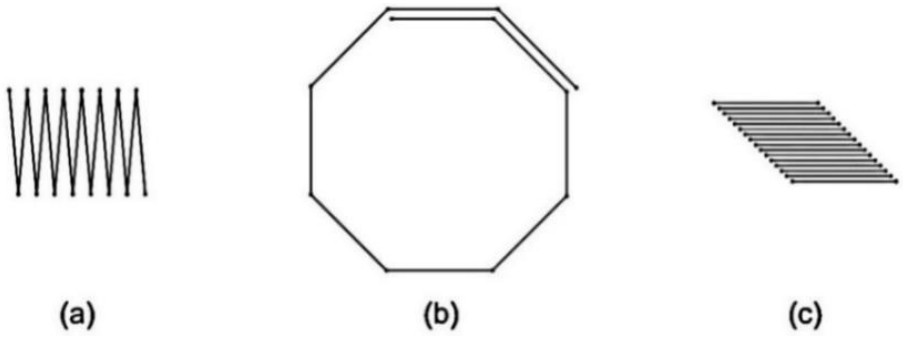

Figure 2.6 - Types of one dimensional folding arrangements (a) Zigzag folding (b) Rollup folding (c) Telescopic Folding

2.4 Geometric Effects of Membrane Thickness

Consider two plates that are connected through a hinge and folds together for stowage. In the simplest analysis, these two plates can be idealized to two lines located at the mid plane of each plate as shown in Figure 2.7 (a). This idealized model allow for 180° rotation between the two plates, whereas, in reality either the rotation will be to an angle less than 180° or the plates will fold to 180° with an offset in the centre lines (see Figure 2.7 (b)) through specially designed hinges or by stretching of plates. This effect is prominent in plate type deployable structures (Trautz & Kunstler, 2010).

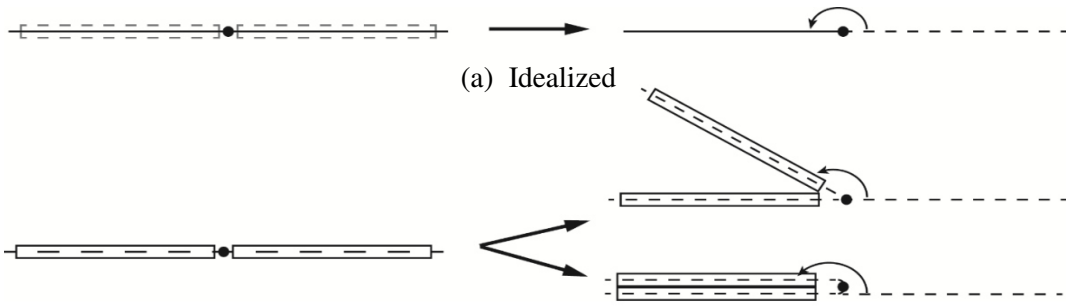

(a) Idealized

(b) Reality

Figure 2.7 - Geometric effects due to plate thickness

Membrane thickness can result in an increase in the required storage, poor repeatability of the stored configuration, and excessive tension/ compression induced on the stored membrane. Excessive tension in the membrane will stretch the membrane plastically causing it to wrinkle once deployed. This is a major issue when it comes to solar sails. IKAROS solar sail demonstrator encountered several problems during the design stage due to membrane thickness (Sakamoto, et al., 2012).

Hence it can be seen that geometric issues caused by the membrane thickness is due to the arrangement of the membrane in the stored configuration and thus can be eliminated by altering the stored configuration by modifying the fold line arrangement. Though membrane thickness can cause issues to all inextensional wrapping patterns, this research focuses on the modification to be carried out for the commonly used spiral folding pattern.

2.5 Simulation of Deployment Behaviour

A vast amount of research has been carried out on deployable structures, where a wide majority of them has been based on physical experiments. Computer based simulations are not common and very little research on approaches to model deployable structures in a virtual environment is available.

Liyanage & Mallikarachchi (2013; 2015) has come up with a basic approach to model the deployment behaviour of membrane type strucures using the commercial FE analysis software Simula Abaqus. In these research two folding patterns: spiral and circumferential folding patterns, which have similar forms has been compared with the use of computer based simulations. Figure 2.8 shows the fold line arrangement of the models used in these research. These research give the basic approach for FE models developed in the current research.

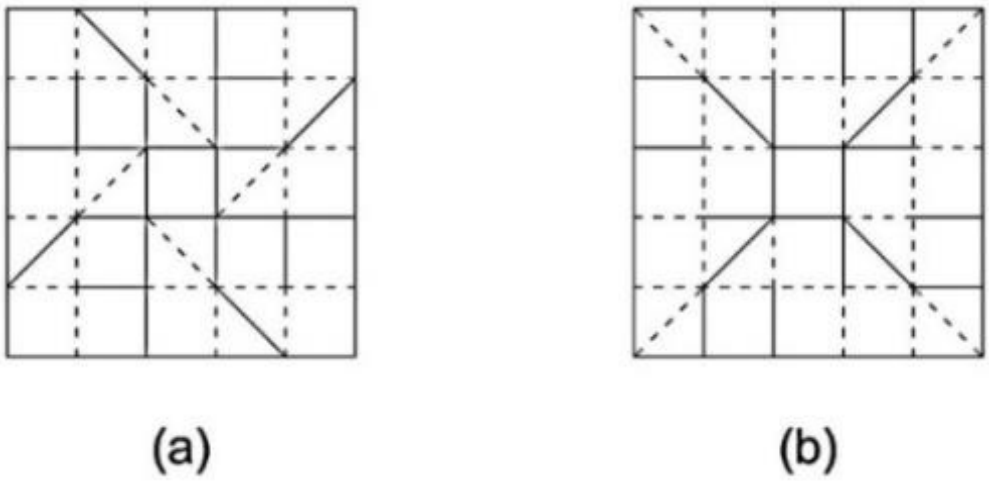

Figure 2.8 - Models used for simulation
(Liyanage & Mallikarachchi, 2015)
(a) Spiral folding pattern (b) Circumferential folding pattern

Liyanage & Mallikarachchi (2013; 2015) compared basic level models of two folding patterns based on their deployment behaviour and energy requirements. Each model had square shaped membranes of 50 mm × 50 mm made from Mylar with a thickness of 10 μm, which wrapped around a square shaped hub of 10 mm × 10 mm.

Models were made in the folded state by attaching square and right angle isosceles triangular shaped shell elements by tie constraints as necessary. These elements were later meshed to comprise smaller quad (S4) elements. Each model consists of 3513 nodes and 2900 (S4) elements with the dimension of an element being around 1 mm (see Figure 2.9). These elements were allows to rotate freely at the ties without any resistance.

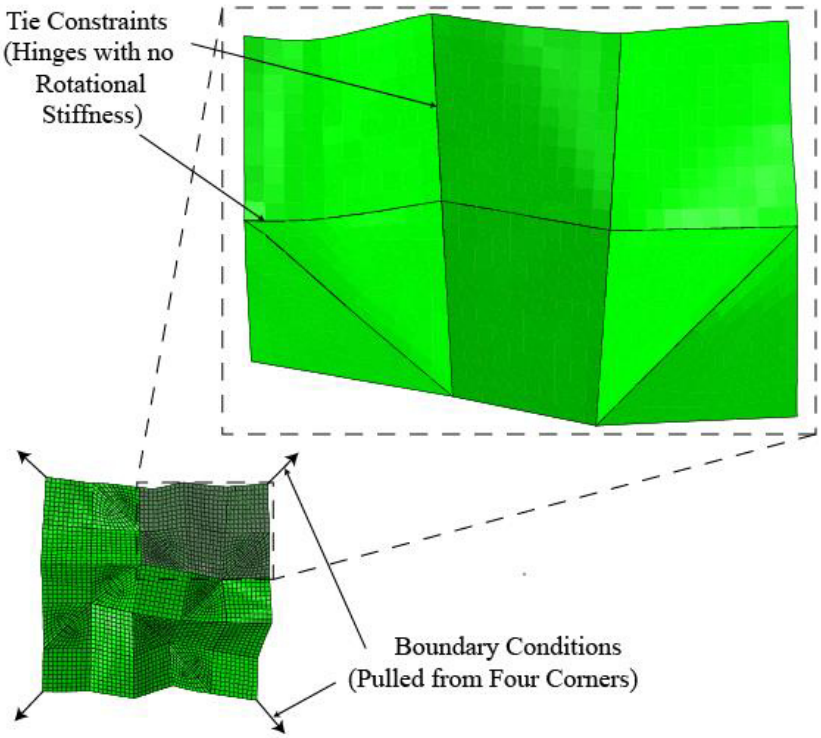

Figure 2.9 - Abaqus model for spiral folding pattern (Liyanage & Mallikarachchi, 2015)

Deployment of these models were provided by a displacement boundary condition which pulls the four corners of the membrane in the radial direction, with a gradual increase and decrease in the velocity at the start and the end respectively to avoid sudden jerks, until the fully deployed configuration is reached. For the analysis Abaqus Explicit solver has been used.

Liyanage & Mallikarachchi (2013) had some issues in the deloyment of these models, especially for the circumferential folding pattern, where some panels were moving through each other and causing some form of sticking between membrane panels (see Figure 2.10). This issue was resolved by Liyanage & Mallikarachchi (2015) with the introduction of surface contact between selected panels. This approach could cause problems to the arrangement of panels in the model in folded state due to the geometric effects triggered by the thickness of the membrane.

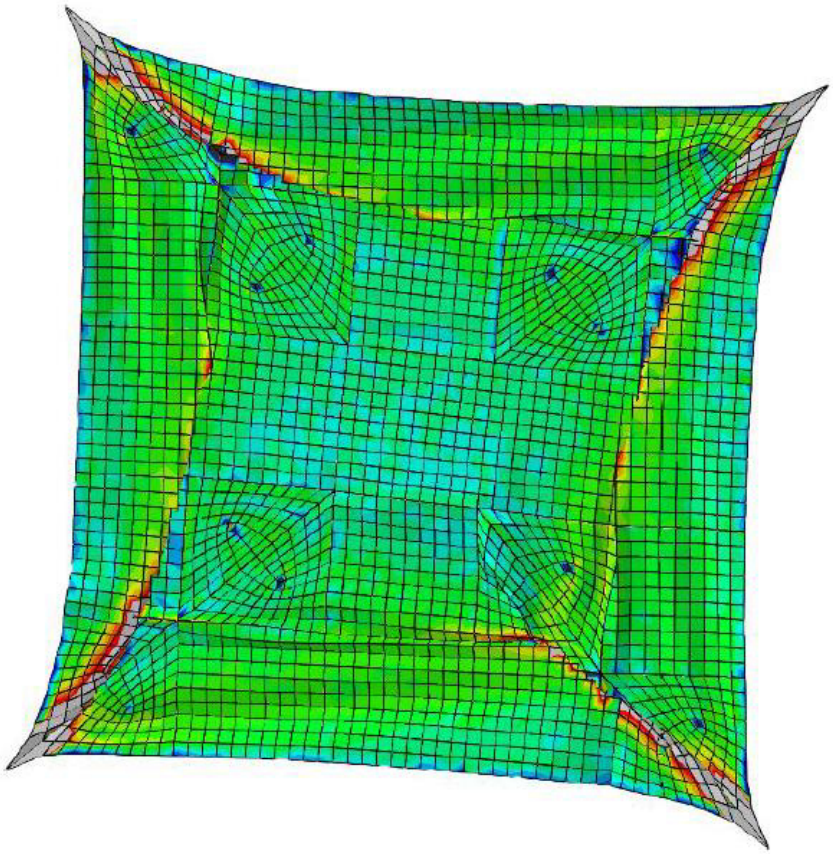

Figure 2.10 - Circumferential folding pattern in the fully deployed state (Liyanage & Mallikarachchi, 2013)

Spiral folding pattern was recommended in both the research because of the smooth deployment behaviour and the low energy requirement (see Figure 2.11).

Both the research had problems with the robustness of the analysis as indicated by the energy plots (see Figure 2.12). The artificial and the total energies of models were not insignificant when compared with the strain energy signifying that models needs to be improved (Liyanage & Mallikarachchi, 2013; 2015).

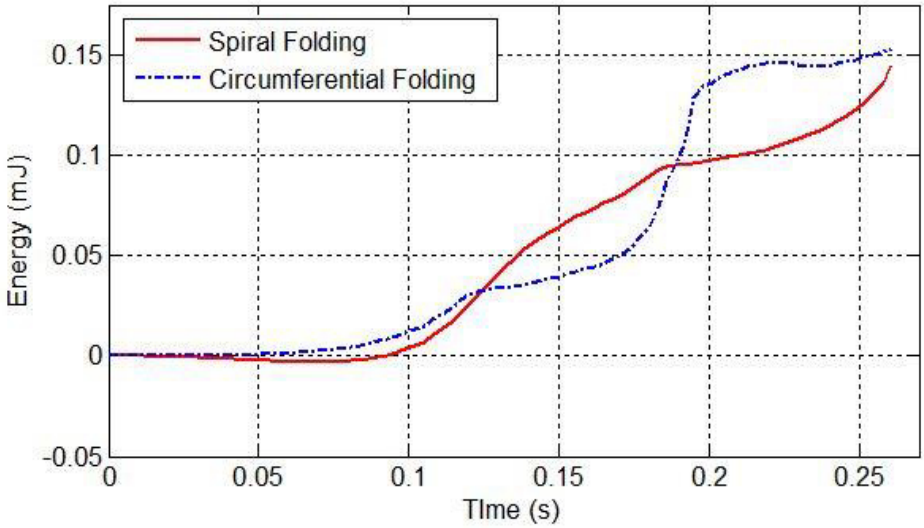

Figure 2.11 - Energy required for deployment (Liyanage & Mallikarachchi, 2015)

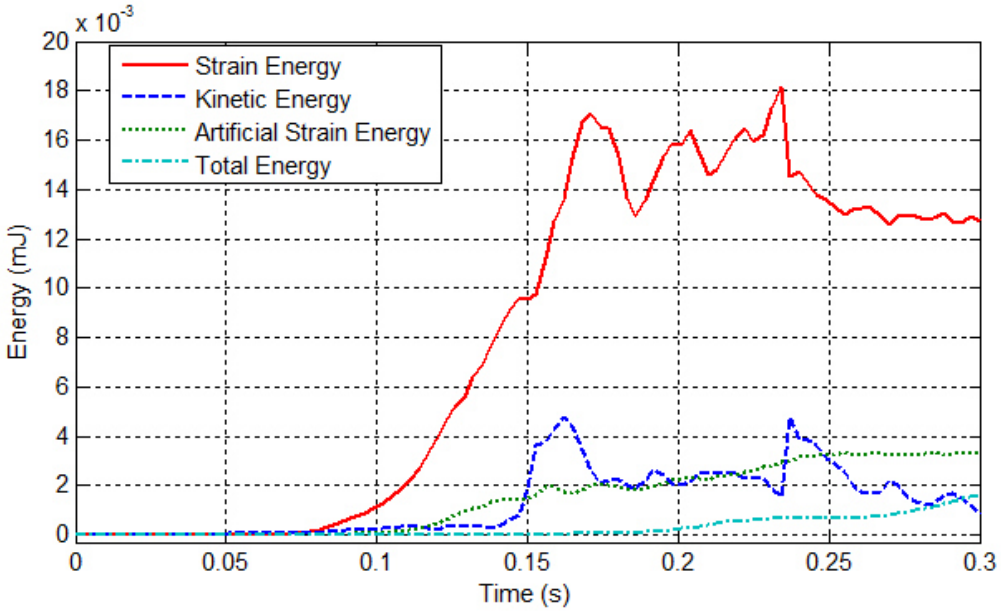

Figure 2.12 - Energy variation of spiral folding pattern (Liyanage & Mallikarachchi, 2015)

All the models in Liyanage & Mallikarachchi (2013; 2015) were idealized on membrane thickness and crease behaviour. Thickness of membranes were ignored when deciding the arrangement of the panels in the folded state, where several panels will be occupying the same space. Creases were modelled as hinges with zero stiffness, which can affect the accuracy of the results as presence of creases can increase the energy required for the membrane to deploy.

2.6 Crease Behaviour

A crease can be defined as a separation line created when a sheet is folded (Amigo & Östlund, 2012). Creasing behaviour is majorly considered in research related to paperboard. Most of these research has been in a micro level considering a single crease and effects of delamination of plies in paperboard, using experiments and FE models (Beex & Peerlings, 2009; Giampieri, et al., 2011; Nagasawa, et al., 2003).

Crease stiffness shows a non-linear relationship with the rotation angle. The moment rotation relationship is similar to that shown in Figure 2.13 (Amigo & Östlund, 2012; Beex & Peerlings, 2009; Giampieri, et al., 2011). Crease stiffness is expected to be dependent on material properties: tensile strength; bending stiffness, opening angle of the crease, folding process, creasing equipment, geometry of the scoring operation and many other unknown factors. But a proper relationship between these properties and the crease stiffness has not been identified (Amigo & Östlund, 2012).

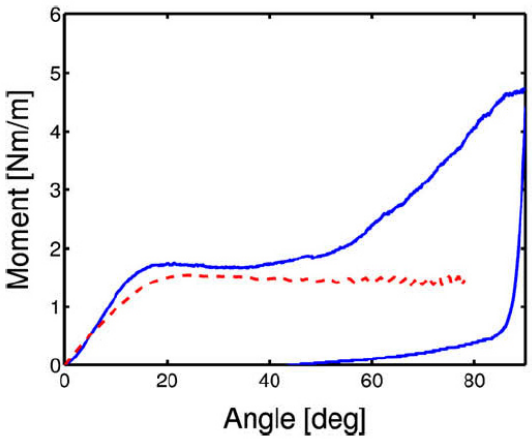

Figure 2.13 - Moment rotation relationship at a cease (Beex & Peerlings, 2009)

Amigo & Östlund (2012) has proposed a technique to model a crease using the FE analysis software Simulia Abaqus, considering a crease as a mean of joining two separate surfaces. This has been used at a macro level, to create a FE model of a paperboard box. It has been consdered that a crease will allow the two adjascent surfaces to rotate around it, while restricting all the other degrees of freedom (DOF) (see Figure 2.14).

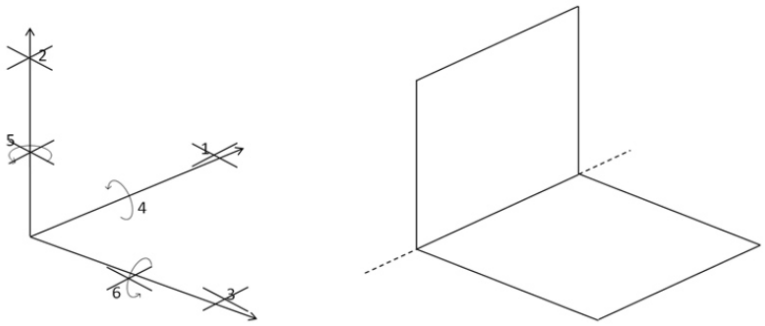

Figure 2.14 - Degrees of freedom at edge between two surfaces (Amigo & Östlund, 2012)

This assumption maybe correct for this research where strains along the creases in a box are negligible for most applications. But in cases where significant strains can be expected, this assumption will result in inaccurate results and issues with the robustness of the analysis.

In modelling creases, Amigo & Östlund (2012) assumes a crease to have a linear spring effect. The FE analysis package used does not have means to model linear springs. Hence, this has been modelled using a collection of rotational springs connecting nodes of the two surfaces as shown in Figure 2.15. In this research, hinge connectors are used which allows the rotation around the axis going through these two nodes, while restricting remaning translations and rotations.

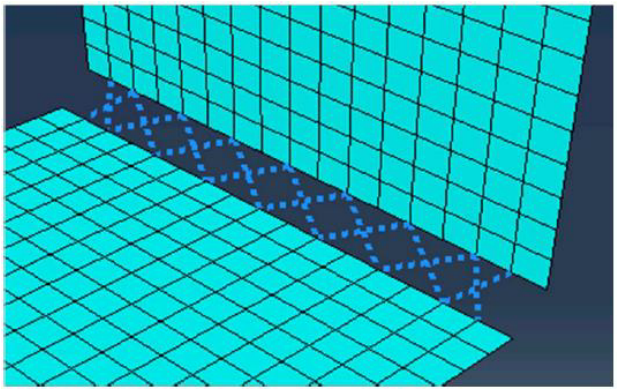

Figure 2.15 - Connectors between two surfaces that form a crease (Amigo & Östlund, 2012)

3 MODIFIED SPIRAL FOLDING PATTERN

Spiral folding pattern described in Section 2.2 is for the idealized folding condition where the thickness of the membrane is assumed to be zero. However in reality thickness of membranes will cause undesirable stretching in the membrane and may cause permanent deformations which will cause the formation of wrinkles in the membrane in the deployed state. As a solution, an approach to eliminate the adverse effects caused by membrane thickness through the modification of the fold line arrangement of the spiral folding pattern was developed. Even though this modification can be extended to model with any polygonal shaped hub, current research is limited for modules with regular polygonal shaped hubs, where rotational symmetry exists, for the sake of simplicity.

Guest & Pellegrino (1992) modified the folding pattern proposed for a solar sail by Temple and Oswald (Cambridge Consultants, 1989) called the tangential folding pattern, so that undesirable stresses caused by membrane thickness in the folded state is eliminated. The modification was carried out by locating nodes (places where fold lines meet) of the folding pattern on vertical planes which passes through the centre of the hub and vertices of the hub, where the offset between two adjacent planes is equal to twice the thickness of the membrane, as shown in Figure 3.1. The modified fold line arrangement was determined by considering vector locations of these nodes in the folded configuration (in a cylindrical coordinate system).

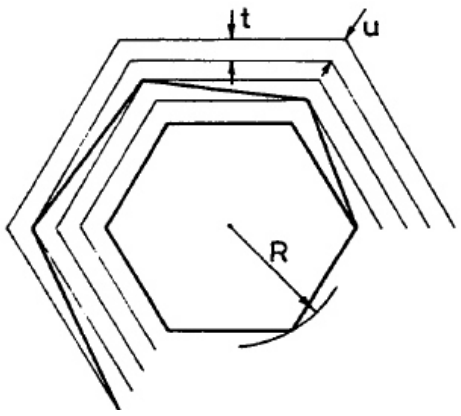

Figure 3.1 - Node arrangement in the folded state for tangential folding pattern (Guest & Pellegrino, 1992)

3.1 Proposed Modification

A similar method was used to modify the spiral folding pattern to eliminate issues caused by the thickness of the membrane mentioned in Section 2.4. Vector locations of nodes were considered in a cylindrical coordinate system, where coordinates were in the form $[r, \theta, z]$ as shown in Figure 3.2.

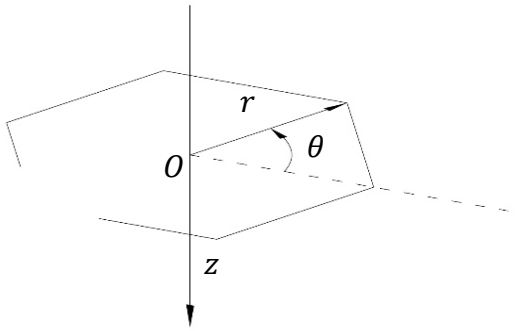

Figure 3.2 - Cylindrical coordinate system

Spiral folding pattern consists of zigzag or Z fold lines (see Figure 2.6 (a)) and rollup folding mechanisms (see Figure 2.6 (b)), where zigzag fold lines starts from each vertex of the hub and goes along similar to a spiral as indicated by red colour lines in Figure 3.3.

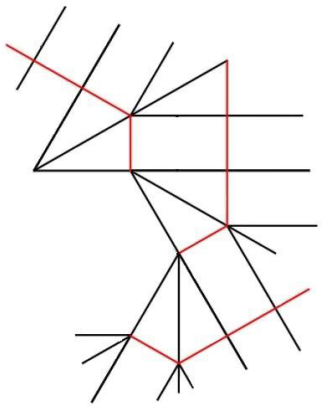

Figure 3.3 - Spiral arrangement around a hub

There will be n spirals in a model with the hub being a polygon with n sides. Once folded, each spirals will cluster at the corresponding vertex of the hub as shown in Figure 3.4. These spirals are connected to each other at node points by lines (black colour lines shown in Figure 3.3) which will wrap around the hub with rollup folding mechanism.

Figure 3.4 - Folding of a single spiral

For convenience of calculations, the nodes were numbered in the format $P_{i,j}$ where "i" is the number assigned to the spiral and "j" is location of the node along each spiral starting with 0 at the vertex of the hub.

It was taken that in the wrapped configuration, each node was located in one of the vertical planes which goes through the centre of the hub and a vertex of the hub. The offset between two adjacent nodes needs to be sufficient to accommodate the thickness of the membrane (see Figure 3.5), i.e. the offset of two adjacent nodes for the model shown in Figure 3.5 should be more than $t/\sin\theta$.

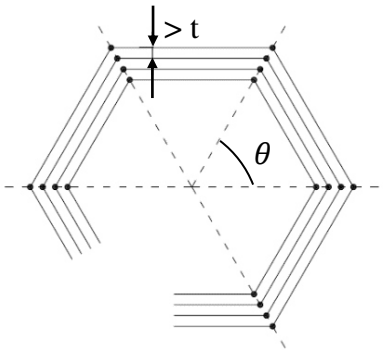

Figure 3.5 - Node arrangement in fully folded state

Considering all the facts mentioned above the general equation, for a pattern with a regular polygonal shaped hub, of the vector location of node $P_{i,j}$ can be written in the form (considering rotational symmetry, see Figure 3.6):

$$P_{i,j} = \left(r_j, \frac{2\pi}{\mathrm{n}}(i-1), z_j\right) \qquad (3.1)$$

Where:

- r_j = Radial distance from the axis passing through the centre of the hub and the j^{th} node in any spiral
- z_j = The z component of the cylindrical coordinate system for the j^{th} node in any spiral
- n = Number of sides in the polygon

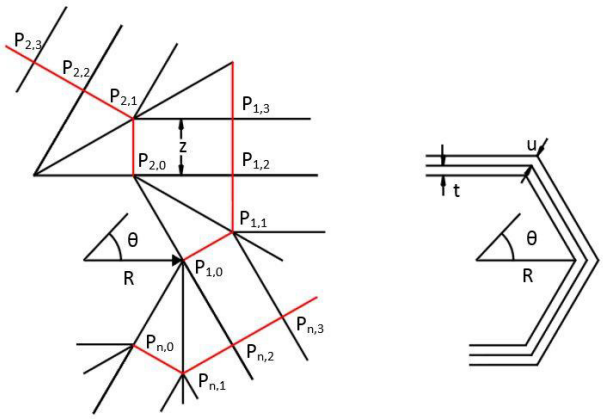

Figure 3.6 - Deployed and folded states of a polygonal shaped module

Finding values for r_j and z_j needs to be done considering two constraints which are required to be met so that the folding pattern can be developed from a plane sheet. First condition is that nodes of quadrilateral elements in the pattern being coplanar, while the second condition is that the sum of angles at a node is equal to 2π.

It can be found that the total number of variables is higher than the total number of constraints. Appropriate values need to be assumed for some of the variables to make the number of variables and constraints the same. Finding r_j and z_j can be done along a spiral starting from zero, where node locations of subsequent nodes will depend on the locations of preceding nodes.

For example let's consider a square shaped module with the fold line arrangement shown in Figure 3.7 where the thickness of the membrane is t.

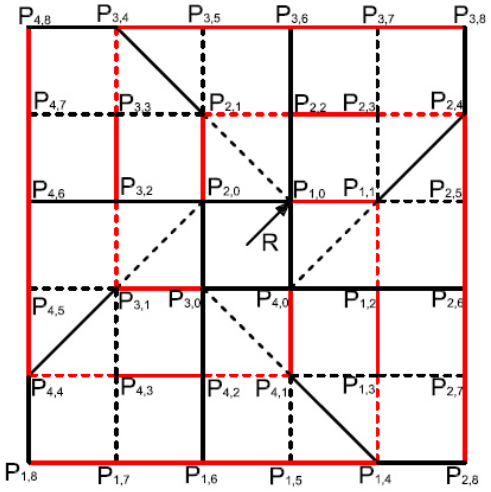

Figure 3.7 - Nodal locations of spiral folding module with a square hub

Vector locations of all the nodes in spiral 1 can be written as shown in Equation 3.2:

$$P_{1,j} = \left(r_j, \pi/4, z_j\right) \tag{3.2}$$

Initially we can assume that:

$$\begin{bmatrix} r_1 \\ r_2 \\ z_1 \end{bmatrix} = \begin{bmatrix} R + \left(t/\cos(\pi/4)\right) \\ R + 2 \times \left(t/\cos(\pi/4)\right) \\ R/\cos(\pi/4) \end{bmatrix} \tag{3.3}$$

Considering the sum of angles at node $P_{1,0}$, the value of z_2 be found.

Then assuming that:

$$r_3 = r_2 + t/\cos(\pi/4) \tag{3.4}$$

z_3 can be found considering the condition for nodes in the quadrilateral $P_{1,0}P_{1,1}P_{2,3}P_{2,2}$, being coplanar.

Two conditions needs to be met when determining location of node $P_{1,6}$. They are: the sum of angles at node $P_{4,2}$ being zero and nodes of quadrilateral $P_{1,5}P_{1,6}P_{4,2}P_{4,1}$ being coplanar.

3.2 Validation of the Proposed Modification

Effect of the proposed modification was investigated by comparing two square shaped models made of paper boards. 0.28 mm thick paper board was selected to enhance the effect of the membrane thickness, in order to provide a better visual representation. R and j were given values 10 mm and 15 respectively. Figure 3.8 (a) and Figure 3.8 (b) show models for folded configurations of the original and the modified spiral folding patterns, respectively. Folding patterns the original folding pattern and the modified folding pattern are attached in Appendix A and Appendix B respectively.

Note that the folded configuration of the model using the original spiral folding pattern takes a shape closer to an oval whereas the shape of the model with the modified spiral folding pattern is closer to a square (see Figure 3.8). Thus the modified folding pattern has improved the overall geometric configuration at the folded state.

(a) (b)

Figure 3.8 - Folded paperboard models with a square hub
(a) Original Folding Pattern (b) Modified Folding Pattern

Careful inspection of nodes at a vertex of the hub in the folded model with the original spiral folding pattern shows that the length of an outer panel is not sufficient to cover the additional lengths added by membrane thickness to the length of an edge of the hub. Hence, there is an accumulated shortfall in the length of fold lines which causes the nodes be located as shown in Figure 3.9 (b). In the case of the model with the modified folding pattern, outer face edges were made longer through the modification and are capable of folding into a square. Further it can be seen that all vertices falls in a straight line as intended (see Figure 3.9 (c)).

(a) (b) (c)

Figure 3.9 - Location of vertices at top right corner
(a) Ideal situation (b) Original folding pattern (c) Modified folding pattern

4 CREASES – BEHAVIOUR AND SIMULATION

Folding a sheet inevitably introduces creases, a permanent deformation, which disturbs the continuity of actions across it. Once created, a crease cannot be undone even how much it is stretched. Behaviour of a crease is different to the planer portions of the sheet, where it acts similar to a hinge having a resistance against rotations around it.

4.1 Simulating Crease Behaviour

In simulating crease behaviour, there was an idea to model it like a linear rotational spring (Amigo & Östlund, 2012). It was assumed that in relation to rotations around the crease, remaining rotations and translations are negligible, hence these DOF (see Figure 2.14) are restricted. Amigo & Östlund (2012) has used hinge type connectors (see Figure 4.1) to model this behaviour in Abaqus through connecting several nodes in respective planes as shown in Figure 2.15.

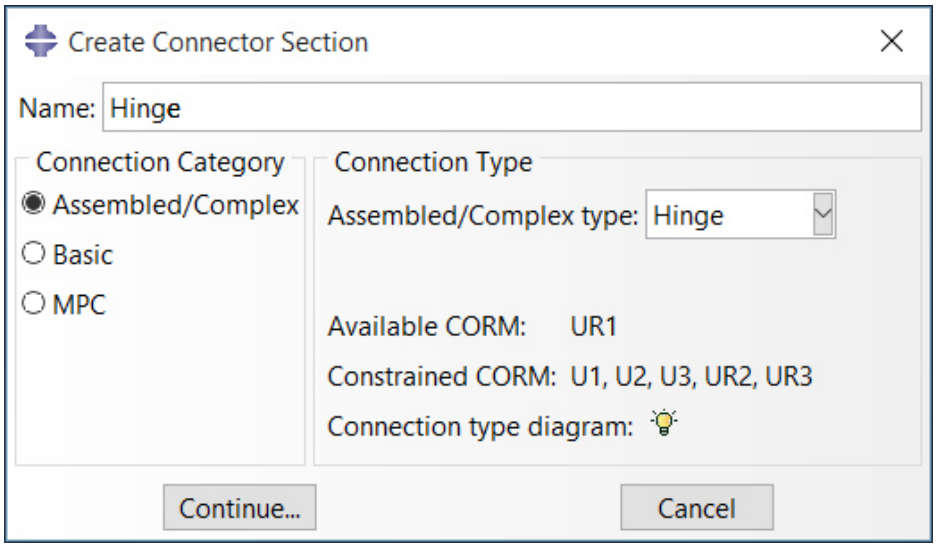

Figure 4.1 - Hinge connector in Abaqus

This assumption maybe valid for the case Amigo & Östlund (2012) considered, where deformations of a paperboard box under different loading condtions were simulated. Deformations in the other directions (specially axial deformations along the axis of the crease) may be insignificant. Hence, restricting these DOF can be justified. But for applications such as deployable structures, where siginficant strains can be expected

along crease lines, this approach may give inaccurate results and cause issues with the robustness of the analysis.

Therefore, a connector which does not restrict any DOF/components of relative motion (CORM), while providing a stiffness for rotations around the crease needs to be used. Cardan type connector was selected as shown in Figure 4.2.

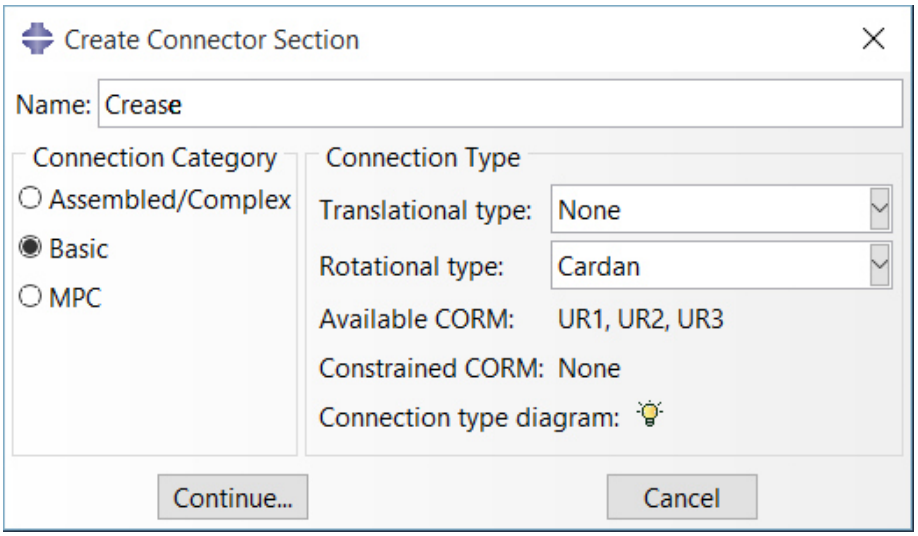

Figure 4.2 - Connector used for simulations

4.2 Crease Stiffness

Since no relationship is available to determine the crease stiffness from the material properties, it was found using an experiment carried out at the Space Structures Laboratory of California Institute of Technology to check the behaviour of creases in 25 µm thick Kapton Polyimide film.

Data from this experiment were used to obtain the crease stiffness in a trial and error manner by matching the deformed shapes of film with FE models created using Abaqus.

In the experiment two inch (50.25 mm) wide strips folded with three creases as shown in Figure 4.3 were loaded with 0 g, 2.25 g, 4.36 g, and 6.09 g weights respectively. Deformed patterns were measured with the use of digital image correlation (DIC). The film used has a thickness of 25 µm, and the material properties are as shown in Table 4.1.

Table 4.1 - Material properties of Kapton Polyimide films

Property	Value
Density	1.42×10^{-9} tonnes/mm^3
Young's Modulus	2500 N/mm^2
Poisson's Ratio	0.34

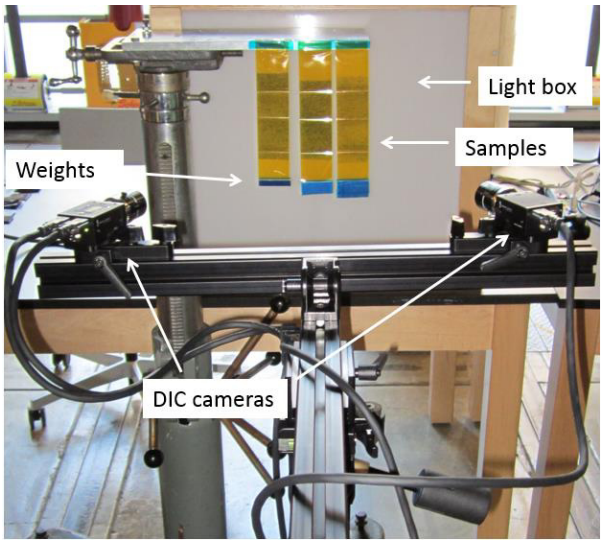

Figure 4.3 - Experimental setup to determine crease behaviour

It was assumed that crease stiffness is linearly proportional to the opening angle of membranes. But in reality it has a more complicated variation as shown in Figure 2.13.

Dimensions and locations of the creases in the Kapton film strip are as shown in Figure 4.4.

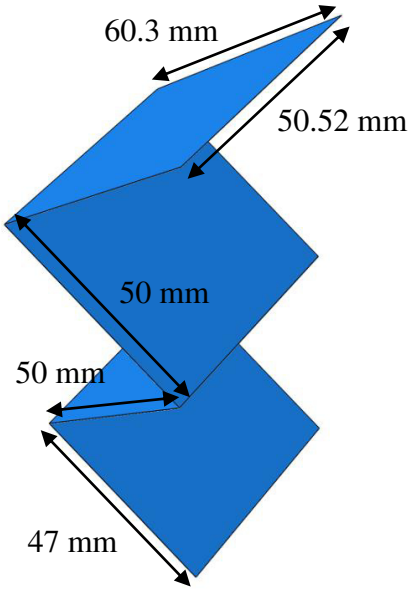

Figure 4.4 - Dimensions of the film

Once the strips were loaded they deformed with a kinked shape at creases (see Figure 4.5) due to the resisting moment developed by crease stiffness. The angle between the adjacent plane sections at a crease is defined as the crease angle.

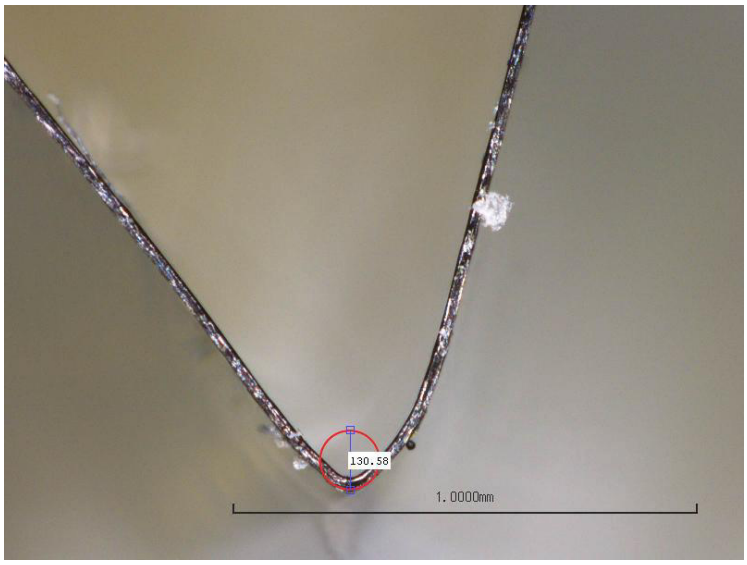

Figure 4.5 - Kink shape at the crease

After applying the load, and allowing the load to stabilize, deformed shape of films were recorded. Crease angles for each specimen was measured using these data. The average crease angles for each load were as shown in Table 4.2.

Table 4.2 - Crease angle variation with loading

Load (g)	Average Crease Angle (°)
0	61
2.25	115
4.36	146
6.09	153

Four rectangular shaped shells were connected at crease locations using tie constraints and cardan connectors to create the FE model. Length of each connector was 6.315 mm, and there were two overlapping connectors between two nodes (see Figure 4.6). Applied loads were modelled by adding vertical loads in the downward direction at the bottom edge of relevant shells. Gravity load was assigned to simulate the self-weight of the membrane. Analyses was done with the standard static general solver.

Figure 4.7 shows the initial state, intermediate stage of deployment, and fully deployed state of the Kapton Polyimide film.

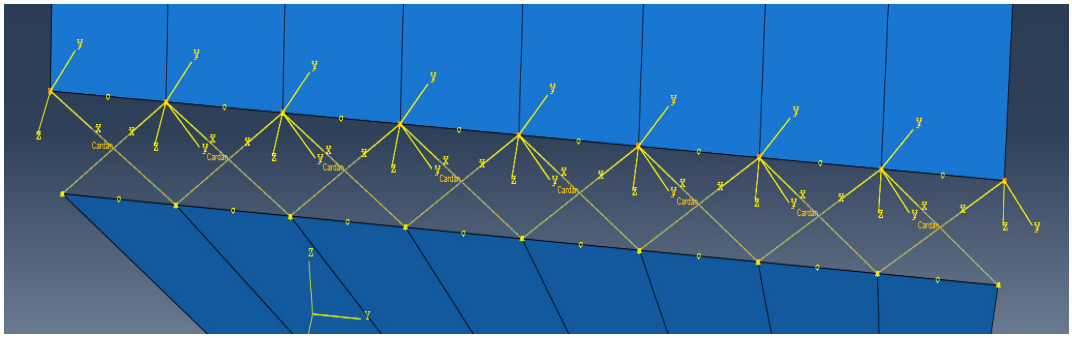

Figure 4.6 - Connector arrangement at a crease

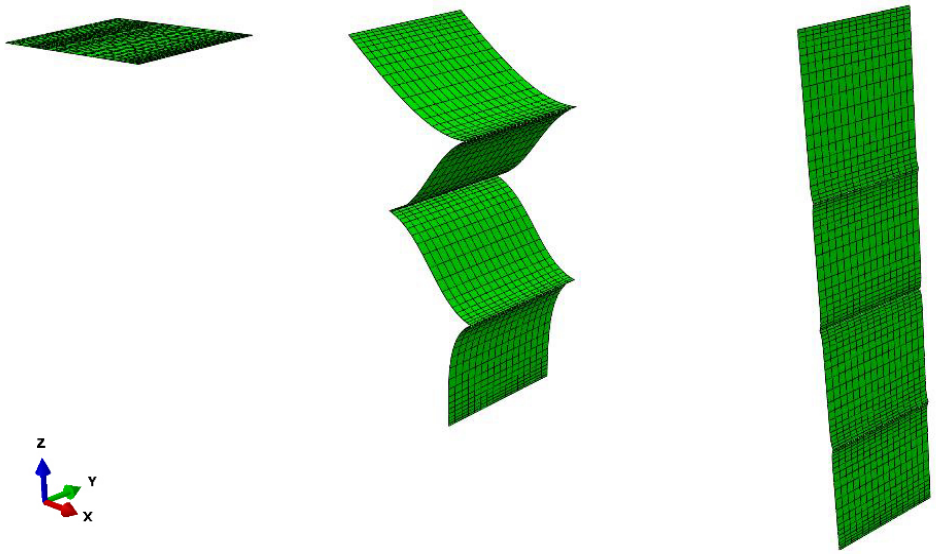

(a) (b) (c)

Figure 4.7 - Loading of the Kapton film
(a) Initial state (b) During loading (c) Fully Deployed State

To get an initial value for the trials, a crease stiffness was obtained for the 4.36 g load by an approximate manual calculation for the crease stiffness. In the film strip loaded with 4.36 g, the average crease offset was recorded as 1.04 mm. Hence the resisting moment at a crease will be 0.0445 N mm ($4.36 \times 9.81 \times 10^{-3} \times 1.04$).

Each crease of the model was will be divided to eight parts (see Figure 4.6) of 6.315 mm length giving a resisting moment of 0.00278 N mm (0.0045/8). Under this stiffness, two planes will rotate an angle of 146˚ (2.548181 radians), giving the crease a stiffness of (0.00109 N mm/radian).

This value was used as the initial value for the trials in determining the crease stiffness.

Crease stiffness (or connector stiffness) was varied, while keeping all other properties constant, until the relevant average crease angle for each loading case is met in the fully deployed state.

A cross section of the deformed shape of a FE model follows the pattern shown in Figure 4.8.

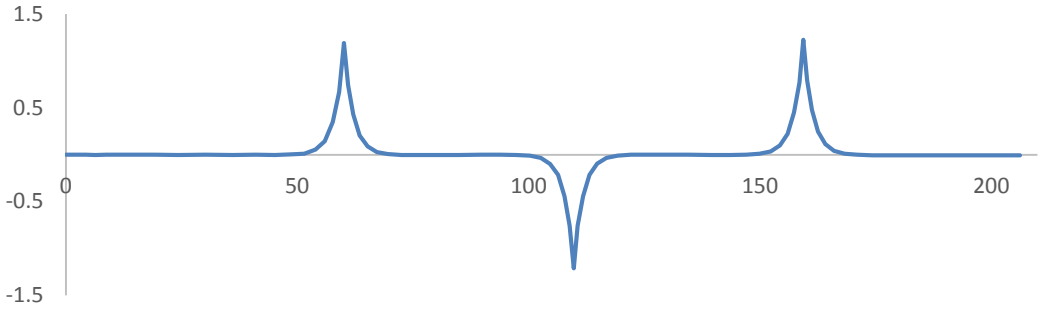

Figure 4.8 - Section profile of the deformed shape of a model

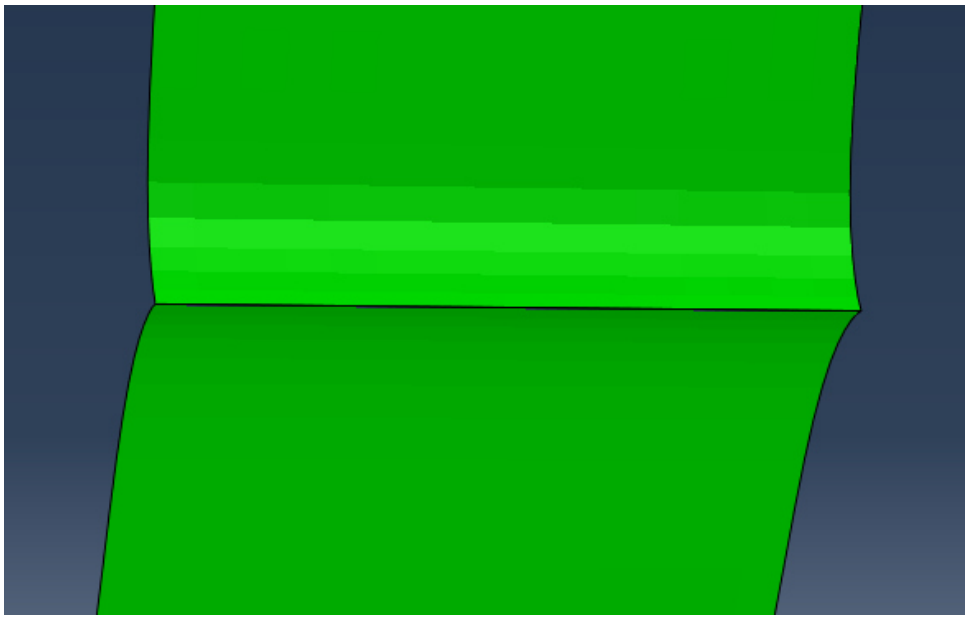

Figure 4.9 - Kinked shape at the crease

For each loading condition, the crease stiffness values (for a 6.315 mm length) were obtained. Table 4.3 shows stiffness values obtained for creases having a length of 6.315 mm, and the resisting moment developed at respective creases.

Thereafter the moment rotation curve for a crease was developed as shown in Figure 4.10.

Table 4.3 - Crease stiffness and resisting moment for the Kapton film

Load (g)	Rotation Angle (Radian)	Crease Stiffness (N mm/ Radian)	Resisting Moment ($\times 10^{-3}$ N mm)
0	1.0647	0.0027	2.8746
2.25	1.9984	0.0040	7.9936
4.36	2.5482	0.0023	5.8608
6.09	2.6704	0.0022	5.8748

The value obtained for the model with a load of 2.25 g was significantly higher than the remaining values. This was taken as a possible error during the experiment and taken off when determining the crease stiffness.

From Figure 4.10, crease stiffness was obtained as 0.00228 N mm/ radian for the crease portion which has a length of 6.315 mm. Since crease stiffness varies linearly with the length, a connector with 1 mm length was take to have a stiffness of 1.81×10^{-4} N mm/ radian (there will be two overlapping connectors per each 6.315 mm long section).

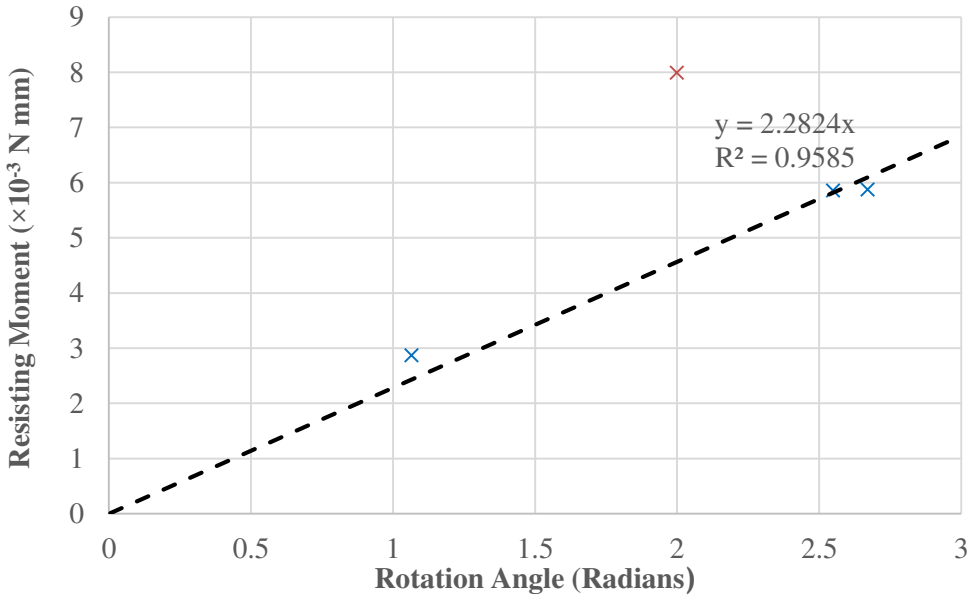

Figure 4.10 - Moment-rotation curve for the crease

5 FINITE ELEMENT MODEL

Deployment and folding of deployable structures are generally identically reversible processes. Hence simulation of either folding or deployment will be adequate to interpret both processes. Due to the convenience of simulation, the deployment behaviour of the modified spiral folding pattern is investigated.

The FE model discussed in this section is of a membrane type deployable structure made from Kapton Polyimide films, folded with the spiral folding pattern modified as discussed in Chapter 3. This deployable membrane wraps around a square shaped hub of 10 mm × 10 mm and has 8 nodes in a single spiral (j = 8, see Figure 3.6).

5.1 Modelling Technique

Basic methodology followed in making the FE model was to have a collection of discrete panels: a square shaped hub; 16 quadrilateral parts; and 16 triangular parts, connected at the fold lines as shown in Figure 5.1. The model was made in the folded configuration. Then all four corners were pulled until the model was fully deployed.

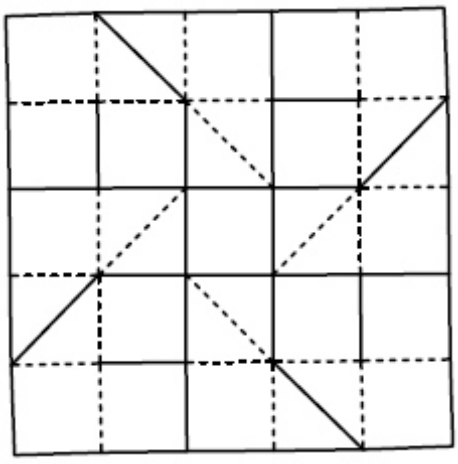

Figure 5.1 - Model used for simulation

These panels were modelled as S4 type shell elements in explicit element library (see Figure 5.2). Quadrilateral and triangular parts were meshed as shown in Figure 5.3 (a) and (b) respectively. All part has a thickness of 25 μm through its section properties. Kapton Polyimide films have the same properties discussed in Table 4.1.

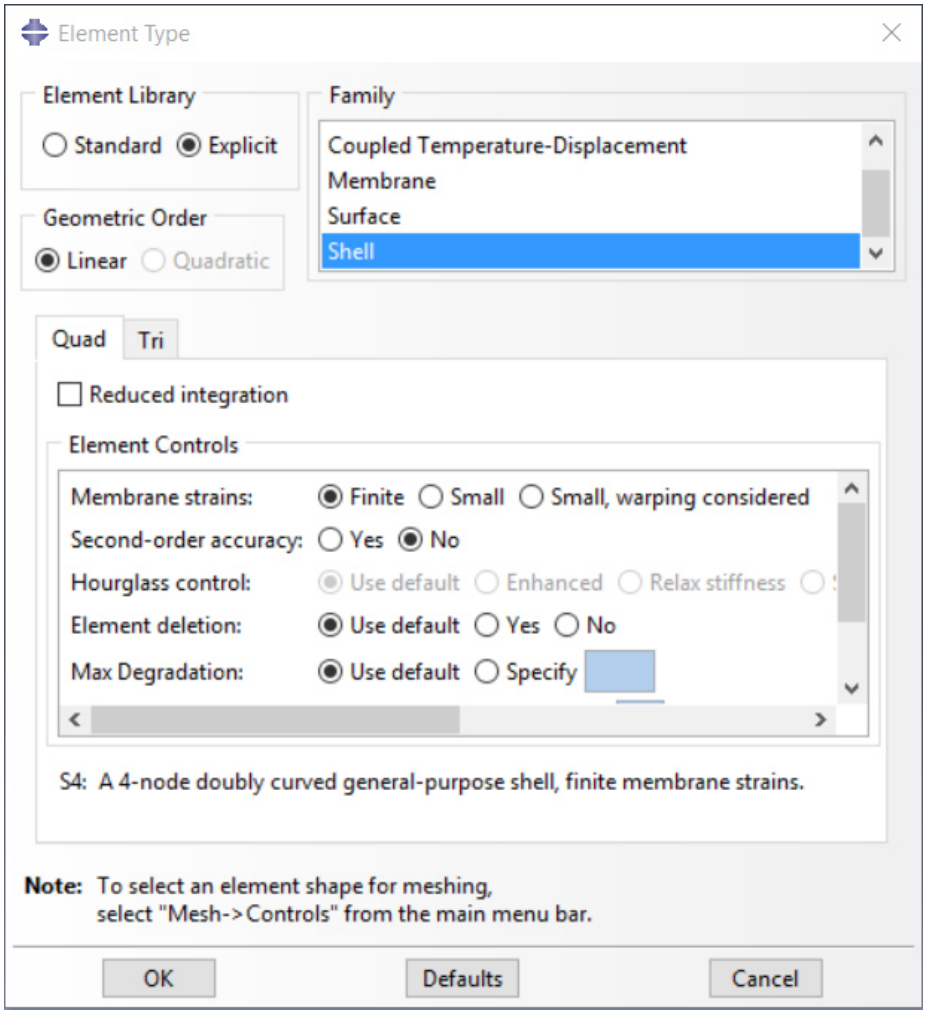

Figure 5.2 - Element type used

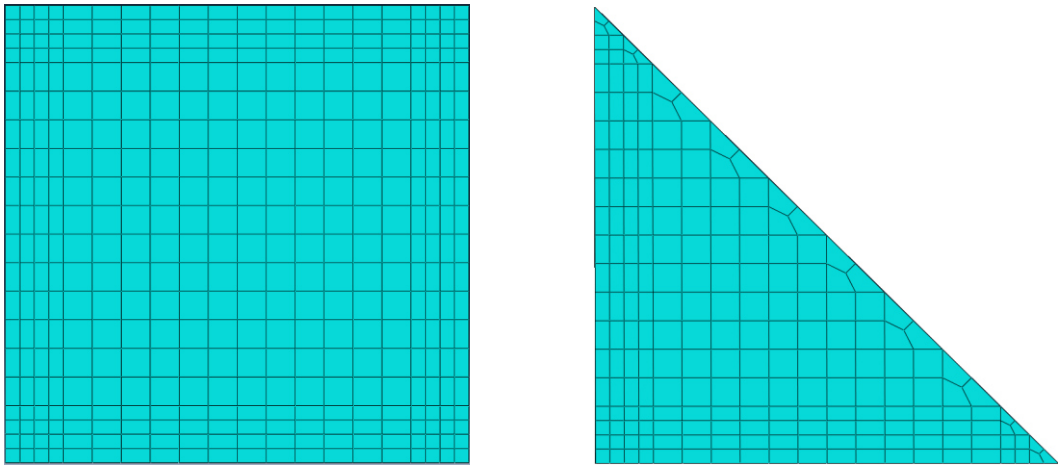

(a) (b)

Figure 5.3 - Meshed parts
(a) Quadrilateral parts(b) Triangular parts

These parts were assembled in the storage configuration and connected together by tie constraints (see Figure 5.4), to restrict the relative translations between two connected parts, without restricting rotations around creases. Connectors were used to model the stiffness of creases. Nodes of two connected panels were bonded by Cardan type connectors (see Figure 4.2) which acts like a linear rotational spring (see Figure 2.15).

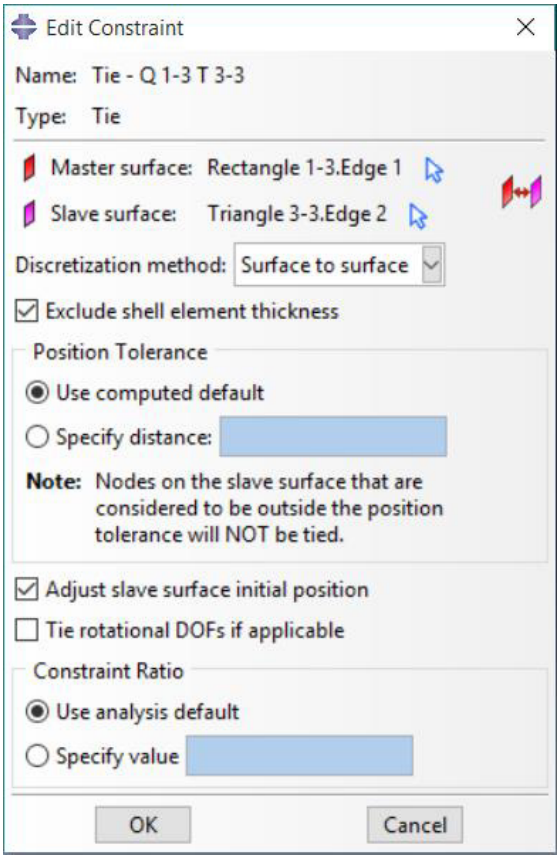

Figure 5.4 - Tie constraints

It has been found that crease stiffness varies linearly with the length of a connector (Amigo & Östlund, 2012). Hence depending on the length of the connector the stiffness value included needs to be changed. Rotational stiffness of a connector is given in the format resisting moment/radian.

Boundary conditions were used to provide the deployment, which displaced the four corners of the model in the radial direction (see Figure 5.5), until the model is fully deployed. Deployment was done with a in a smooth step function (see Figure 5.6). This type of function is used to avoid sudden changes in the velocities.

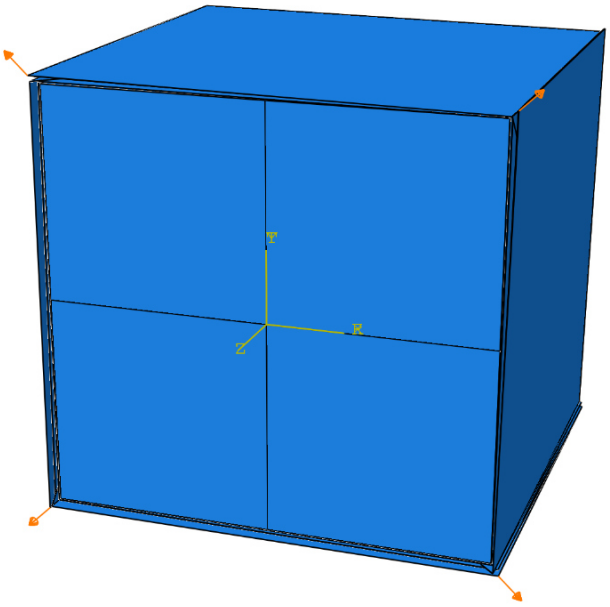

Figure 5.5 – Deployment of the model

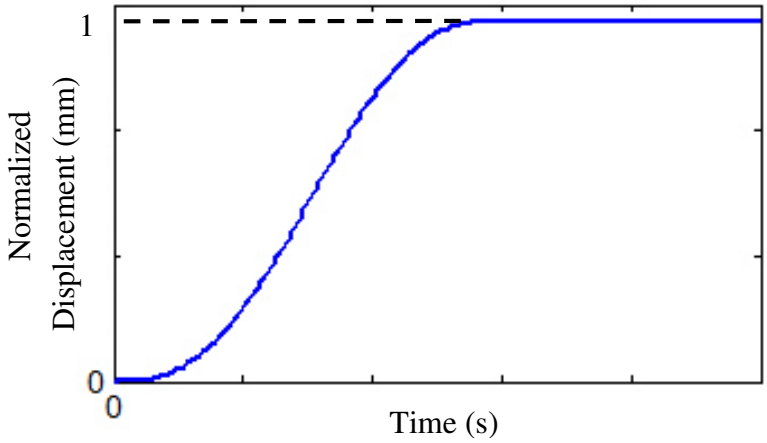

Figure 5.6 - Displacement vs. Time

Results of the analysis carried out are discussed in the next chapter.

5.2 Abaqus Explicit Solver

Folding and deployment of ultra-thin structures are accompanied with significant geometric changes such as: instabilities; dynamic snaps; and extensive contact/sliding. Issues with numeric instability, convergence associated with the singularity in the stiffness matrix has limited the number of folds, etc. in previous studies. As a solution, an explicit solver which avoids the stiffness matrix and uses equations of motion to

find the next state from already available data (Mallikarachchi, 2011). Abaqus explicit solver provides an explicit solver, which is used in this research as sudden changes in the structures behaviour such as dynamic snapping were expected in simulations.

Explicit solvers keep the time increment at a very small level. To artificially increase the time step of the analysis, mass scaling is used, where the mass of elements having a value below a threshold value is increased. If the mass of an element is increased by a factor of k, the time step of that element will increase by a factor of $\sqrt{k}$. This can affect the accuracy of an analysis, but for quasi-static analysis, the effect will be low.

As a check for the robustness of an analysis, energy histories can be used, especially the energy balance/total energy (E_b), which is defined by Equation 5.1.

$$E_b = E_i + E_v + E_k - E_w \quad (5.1)$$

Where, internal strain energy E_i includes the sum of strain energy and the artificial strain energy, E_v is the viscous dissipation, E_k is the kinetic energy, and E_w being the sum of work by all external forces (Mallikarachchi, 2011).

Artificial strain energy is the energy built-up by the solver in preventing uncontrollable deformations. Artificial energy being approximately greater than 1 % of the strain energy is an indication of excessive hourglassing effect, which would mean that the mesh and the element types of the model needs to be modified (Lempiäinen, 2008).

The energy balance should remain equal to the energy introduced to the structure throughout the process as the energy stored and dissipated within the system should be constant. If there are significant variations to the total energy, that would indicate some serious issue in modelling.

In practice these structures are deployed in a quasi-static manner. Thus selecting a suitable time step is quite important in simulating quasi-static conditions accurately. This can be done by maintaining the kinetic energy of the model to be less than 1 % of the strain energy during the simulation (Dassault Systémes Simulia Corp., 2012). However kinetic energy can have a higher value when it comes to dynamic snapping.

6 RESULTS AND DISCUSSION

Main objective of the research is to develop a high fidelity simulation technique to predict the deployment behaviour of membrane type deployable structures using FE models. Starting from a basic level FE model of the spiral folding pattern several improvements were made to get better results from the analysis.

6.1 Modified Spiral Folding Pattern

Initially a technique was developed to modify the fold line arrangement of the spiral folding pattern so that the adverse effects of caused by the membrane thickness such as: increase in the required storage; poor repeatability of the stored configuration; and excessive tension/ compression induced on the stored membrane, are avoided.

This technique aims to achieve a stress free state both in the fully folded and fully deployed states. The principle behind this was derived from the modification Guest & Pellegrino (1992) did for the tangential folding pattern, where the node arrangements in the folded state was modified, so that the maximum offest between two panels is equal to twice the thickness so that sufficient space is available for storage of the membrane without straining it.

Following a similar approach, a technique was developed by altering the vector locations of nodes so that there is sufficient offest between membrane surfaces for storage and conditions that need to be met to achieve developability of the structure. To obtain a stress free deployed state, two conditions were required to be met, which will develop the model to a flat sheet. The conditions that need to be met are: sum of angles around each node needs to be equal to 2π (360°); and nodes of the quadrilateral members needs to be coplaner.

Using paperboard models of 0.28 mm thickness, the modification technique was verified for a square shaped model with R and j were given values 10 mm and 15 respectively. Figure 3.9 shows the node arrangement for the modified and the original

folding patterns, where the model with the modified pattern shows straighter lines with less stresses developed, which indicates that the modification is successful.

6.2 Crease Stiffness

Creases are formed when a sheet is folded, which will alter the behaviour of the sheet especially around the crease. There are two main features of a crease which were identified: resistance against rotations around the crease; and permanent deformation along the crease line. An idea to model this was to have a linear rotational spring along the crease having a certain stiffness. Since no proper relationships are available to determine the crease stiffness based on material properties and/ or any other features, crease stiffness needs to be determined experimentally.

As the model to be simulated is made from Kapton Polyimide film, stiffness of a crease created in Kapton Polyimide film needs to be determined. This was determined from an experiment carried out in the Space Structures Laboratory of California Institute of Technology to measure crease behaviour, where several 2 inches wide Kapton film strips were suspended by pinned connection from one end and different loads were applied at the other end.

The deformed pattern of these patterns were recorded using DIC, and the average crease angles for each model was obtained from them. FE models made from Simulia Abaqus were used to model this behaviour, where crease stiffness was modelled using Cardan type connectors.

With a trial and error process, the crease stiffness was found for each model and a moment rotation curve was developed (see Figure 4.10). In these models the connector stiffness was varied, while keeping all the other parameters constant. From the four results, one value shows great mismatch with the other values, and hence was taken off when developing the moment rotation curve. The curve showed that the moment rotation relationship is approximately linear. Then the crease stiffness was obtained as 0.00228 N mm/ radian for a crease length of 6.315 mm, which gives a stiffness value of 3.62×10^{-4} N mm/ radian for a crease of 1 mm length.

During the analysis, the deployment (see Figure 4.7) needs to be done slowly to match the conditions of the test and avoid any impact loads which could alter the behaviour of a crease. Hence a static general type loading step was defined, where automatic viscous damping is used to stabilize the model.

Figure 6.1 shows the variation of strain energy, kinetic energy, artificial energy, and total energy with the vertical displacement of the loaded edge. Comparative to the strain energy, all the other energies are insignificant, which shows that the deployment can be classified as a quasi-static deployment process and the analysis has been carried out accurately.

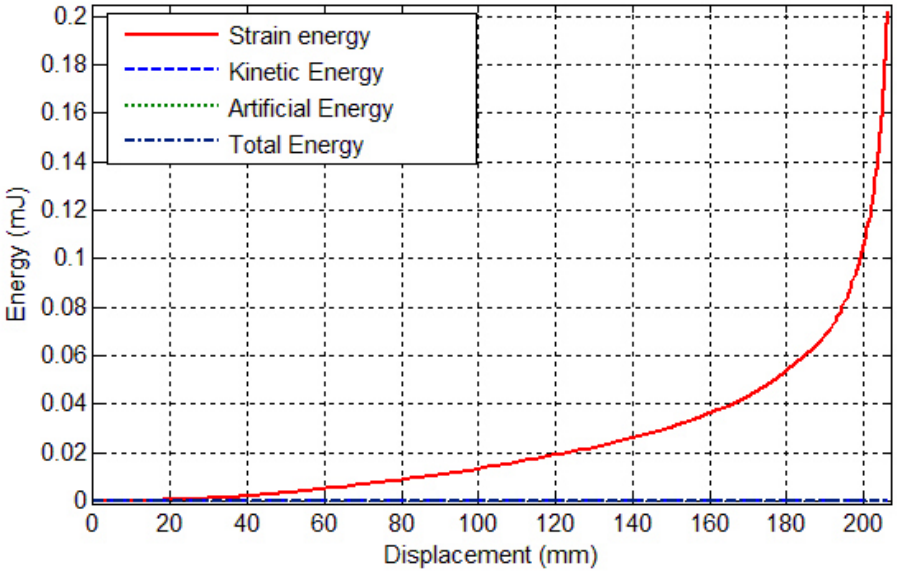

Figure 6.1 - Energy history of a Kapton film simulation

6.3 Simulation of the Finite Element Models

This section discusses the results of the FE analysis carried out for two models folded with the modified spiral folding pattern: with and without crease stiffness. Effects on deployment from the crease behaviour and other significant features of the analysis are looked here.

Figure 6.2 shows the energy variation for the FE model with the radial displacement of a corner of the module, which has creases with zero stiffness. Here the deployment was done in 4 s, at an average rate of 7 mm/s, a relatively slow rate. But the kinetic

energy was significant with respect to the strain energy, and sometimes even higher than it. Hence this cannot be classified as a quasi-static deployment process.

Approximately after 3 mm of deployment, there is a spike in the kinetic energy curve which coincides with a decrease in the strain energy. This signifies a dynamic snap in the model where a portion of the strain energy developed in the structure gets released as kinetic energy. This kinetic energy has caused the structure to vibrate which is indicated by the small variations in the strain and kinetic energy curves after the occurrence of a snap.

Generally a major portion of this kinetic energy will get dissipated by the stiffness provided at creases, acting as an internal damping mechanism against vibrations. Since the crease stiffness is not available, these vibrations will continue to exist for a long time.

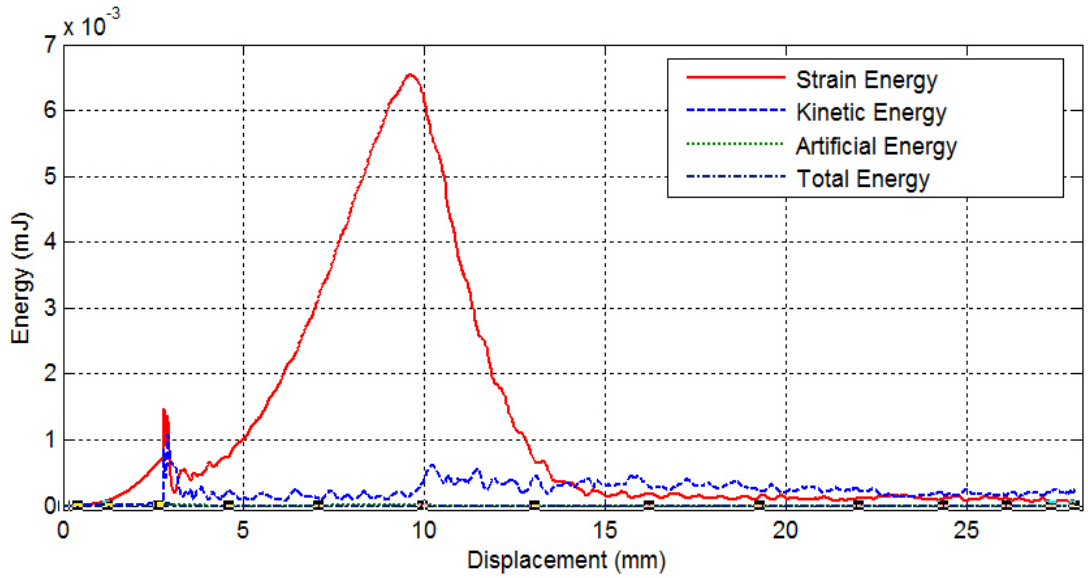

Figure 6.2 - Energy history for the FE model without crease stiffness

At about 10 mm of deployment, the peak strain energy is reached, and then comes down until it is very small. This is expected in these type of structures, where the fully folded, and fully deployed states are stress free. The artificial and the total energy values are insignificant with respect to the strain energy which indicates that the analysis was carried out without any errors.

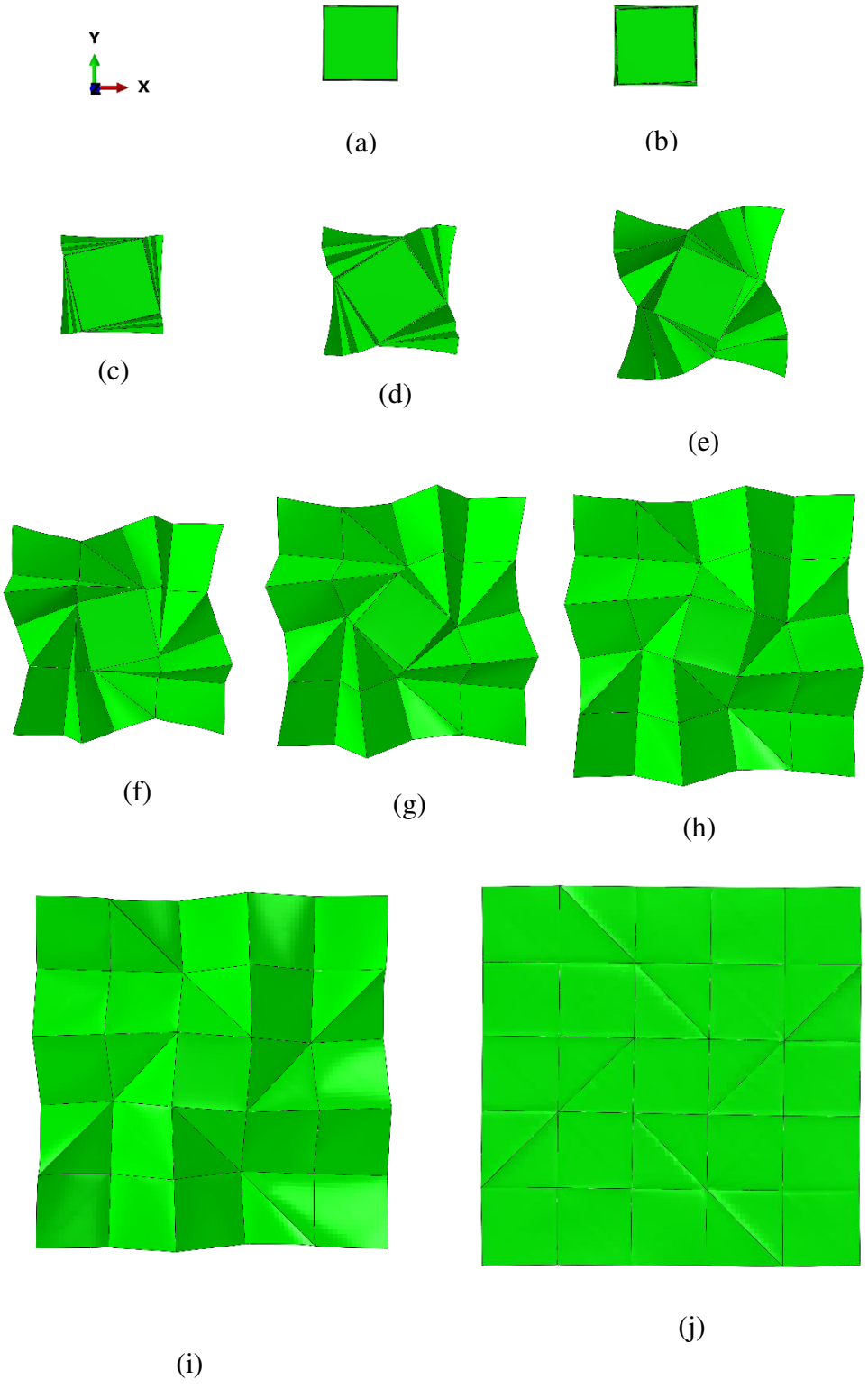

Figure 6.3- Deployment of the model with crease stiffness
(a) Time step 0 s (b) Time step 0.2 s (c) Time Step 0.4 s (d) Time Step 0.6 s
(e) Time Step 0.8 s (f) Time Step 1.0 s (g) Time step 1.2 s
(h) Time step 1.4 s (i) Time step 1.6 s (j) Time step 1.8 s

Similarly the model with crease stiffness was analysed, where the deployment was carried out more rapidly within 1.8 seconds. Even with the faster deployment, the kinetic energy was very low compared to the strain energy, suggesting that this is a quasi-static deployment process. On that aspect this is much closer to a real structure.

Figure 6.3 shows snapshots from the deployment of the model.

Unlike for the previous model, there are no substantial vibrations are present, which might have been damped by the stiffness effect of creases. This model shows much smoother deployment.

Figure 6.4 shows the variation of energy against the radial displacement of a corner of the module. Similar to the previous model, the robustness of the analysis is shown by the artificial and total energy curves, showing no significant variation. This means that the analysis is robust, and no errors are present in the model.

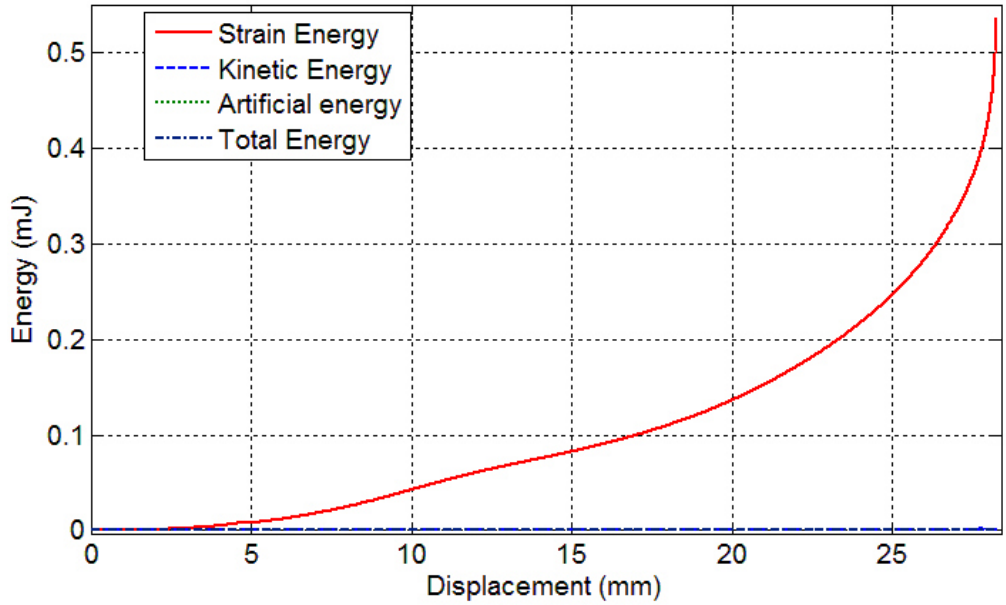

Figure 6.4 - Energy history for the FE model with crease stiffness

The maximum strain energies developed in the first and second models are 6.6×10^{-3} mJ, and 0.53 mJ. The second model has developed approximately 80 times strain more energy than the first model. The additional energy is required to act against the resistance provided at the creases to unfold. This suggest that an analysis without crease properties will give results, significantly different from the actual values.

The resisting force against the displacement of a corner of the module in the radial direction, has an exponential variation with small amount of noise (see Figure 6.5). The maximum force required is about 0.35 N to keep the deployed model in that state.

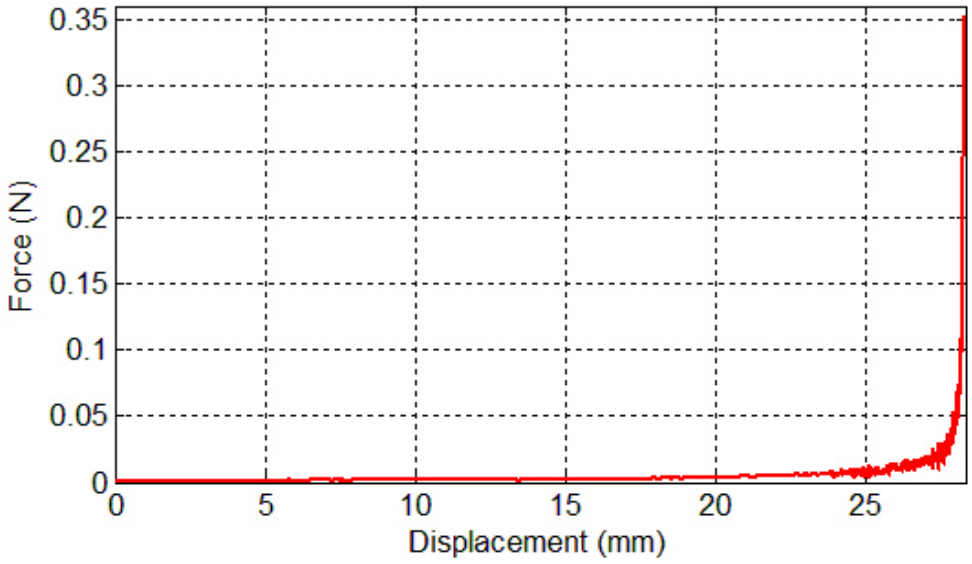

Figure 6.5 - Force Variation displacement time for the model with creases.

For this model the external energy requirement is mainly governed by the strain energy developed in the structure.

7 CONCLUSIONS AND FUTURE WORK

7.1 Modified Spiral Folding Pattern

Neglecting geometric effects of membrane thickness can result in plastic deformations and wrinkling of membranes. As the issues arise in the stored configuration, they can be overcome by certain modifications to the fold line arrangement in the pattern. We have developed a modified fold line arrangement for modules which utilizes the spiral folding pattern using the arrangement of nodes in the folded state, and conditions which will make it possible for the folding pattern to be developed from a plane sheet. The proposed modification was verified using paperboard models for a square shaped module.

7.2 Crease Stiffness

Crease stiffness for 25 μm thick Kapton Polyimide films were found by a trial and error method, by comparing an experiment carried out at the Space Structures Laboratory in California Institute of technology, with FE models developed to match the behaviour.

A moment rotation curve was developed, which shows an approximate linear variation. Then the crease stiffness of 25 μm thick Kapton Polyimide film was found to be 3.62×10^{-4} N mm/ radian for a 1mm long crease.

7.3 Simulating the Deployment Behaviour of Deployable Structures

The deployment behaviour of the modified spiral folding pattern was simulated successfully using the Abaqus FE analysis software. It was found that crease stiffness will have a significant effect on the deployment behaviour and energy requirements.

The simulation for the model with creases showed a quasi-static process, while he model without crease stiffness couldn't be classified as a quasi-static process signifying the importance of crease stiffness on dynamic behaviour.

7.4 Recommendations for Future Work

Even though the crease stiffness was determined, no checks were done on whether the assumption made on linearized crease stiffness variation was accurate enough. An experiment needs to be carried out for the proposed model to check the validity of this assumption and to verify whether the modelling technique proposed can be used to predict the deployment behaviour accurately.

Arya & Pellegrino (2014), has given details from an experiment carried out to check the deployment behaviour of structures made from Kapton film folded with the tangential folding pattern. This can be used as a mean of verifying the crease stiffness as well as the modelling technique.

The model analyzed is of the most simple form which might not include all the behaviours such as dynamic snapping. Hence a model with higher number of folds needs to be checked to see the real behaviour of the structure.

REFERENCES

Amigo, J. C. & Östlund, S., 2012. *Stiffness Design of Paperboard Packages using the Finite Element Method - Master of Science Thesis,* Stockholm, Sweden: s.n.

Anon, 2009. *Hositing the Solar Sail.* [Online] Available at: http://www.rsc.org/chemistryworld/Issues/2009/July/HoistingTheSolarSail.asp [Accessed 25 May 2015].

Anon, 2011. [Online] Available at: http://www.nasa.gov/connect/chat/nanosail_chat2.html#.VFNLmvmUeSo [Accessed 31 October 2014].

Arya, M. & Pellegrino, S., 2014. *Deployment mechanics of highly compacted thin membrane structures.* s.l., s.n.

Beex, L. & Peerlings, R., 2009. An Experimental and Computational Study of Laminated Paperboard Creasing. *International Journal of Solids and Structures,* Volume 46, p. 4192–4207.

Cambridge Consultants, 1989. *Design study for a Mars spacecraft - Technical Report,* s.l.: s.n.

Cubillos, X. C. M. & Souza, L. C. G. d., 2011. *Solar Sails - The Future of Exploration of the Space.* s.l., s.n.

Dassault Systémes Simulia Corp., P. R., 2012. *Manual, Abaqus Users. Version 6.12-1.* s.l.:s.n.

Giampieri, A., Perego, U. & Borsari, R., 2011. A Constitutive Model for the Mechanical Response of the Folding. *International Journal of Solids and Structures,* Volume 48, p. 2275–2287.

Graybeal, N. W. & Craig, J. I., 2006. *Deployment Modeling of an Inflatable Solar Sail Spacecraft.* Keystone Colorado, s.n.

Guest, S., 1994. *Deployable Structures: Concepts and Analysis.* s.l.:University of Cambridge.

Guest, S. & Pellegrino, S., 1992. *Inextensional Wrapping of Flat Membranes.* Montpellier, s.n., pp. 203-215.

Japanese Aerospace Exploration Agency, 2008. *ISAS| Radio Astronomy HALCA (MUSES-B)/Missions.* [Online] Available at: http://www.isas.jaxa.jp/e/enterp/missions/halca/ [Accessed 27 February 2014].

Kishimoto, N., Natori, M., Higuchi, K. & Ukegawa, K., 2006. *New Deployable Membrane Structure Models Inspired by Morphological Changes Nature.* s.l.:American Institute of Aeronautics and Astronautics.

Lang, R. J., 1997. *Origami in Action.* s.l.:MacMillan.

Lempiäinen, J., 2008. Finite Element Simulation of Roll Forming of High Strength Steel.

Liyanage, P. & Mallikarachchi, H., 2013. *Origami based Folding Patterns for Compact Deployable Structuress.* Kandy, Sri Lanka, s.n.

Liyanage, P. & Mallikarachchi, H., 2015. *Folding Patterns for Ultra-thin Deployable Membranes.* Galle, Sri Lanka, s.n.

Mallikarachchi, H., 2011. *Thin-Walled Composite Deployable Booms with Tape-Spring Hinges - Dissertation submitted for the degree of Doctor of Philosophy.* Cambridge: University of Cambridge.

Mori, O. et al., 2009. *First Solar Power Sail Demonstration by IKAROS.* s.l., s.n.

Nagasawa, S. et al., 2003. Effect of Crease Depth and Crease Deviation on Folding. *Journal of Materials Processing Technology,* Volume 140, pp. 157-162.

Natori, M., Katsumata, N. & Yamakawa, H., 2010. *Membrane Modular Space Structure Systems and Deployment Characteristics of their Inflatable Tube Elements.* Orlando, Florida, American Institute of Aeronautics and Astronautics, pp. AIAA 2010-2909.

Pellegrino, S., 2001. *Deployable Structures.* (No. 412): Springer.

Sakamoto, H. et al., 2012. Folding Patterns of Planar Gossamer Space Structures Consisting of Membranes and Booms. *Acta Astronautica,* 94(2014), pp. 34-41.

Schenk, M. & Guest, S., 2011. *Origami folding: A Structural Engineering Approach.* s.l., s.n., pp. 291-303.

Trautz, M. & Kunstler, A., 2010. *Deployable Folded Plate Structures - Folding Patterns Based on 4-Fold-Mechanism Using Stiff Plates.* Valencia, Universitat Politécnica de Valencia.

Warwick, G., 2010. *It Powers as it Sails.* [Online] Available at: http://www.aviationweek.com/Blogs.aspx?plckBlogId=Blog:04ce340e-4b63-4d23-9695-d49ab661f385&plckPostId=Blog%3A04ce340e-4b63-4d23-9695-d49ab661f385Post%3Ad016cf13-caf7-417a-a893-b1a6a9bb5fa0
[Accessed 27 February 2014].

APPENDICES

Appendix A - Original Spiral Folding Pattern Used for Validation

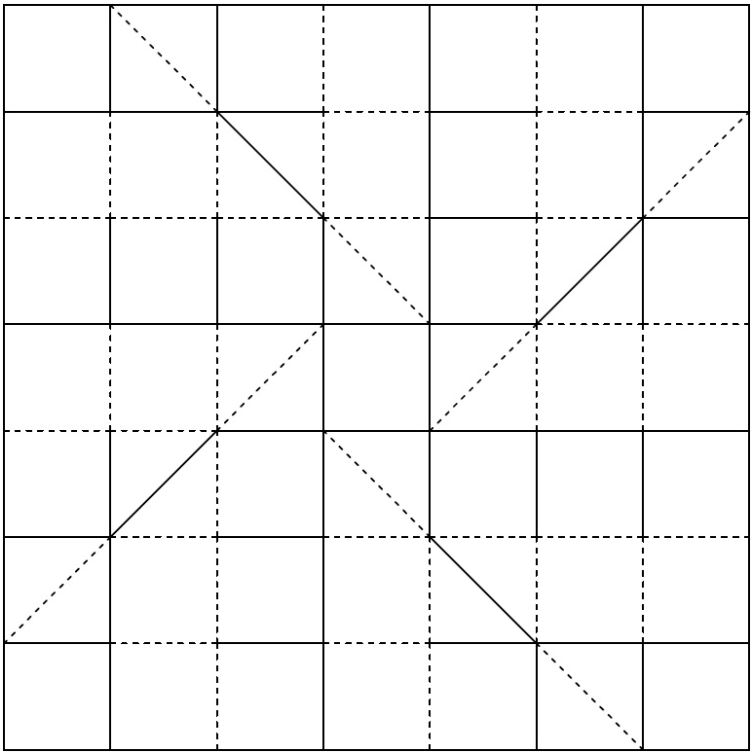

Appendix B - Modified Spiral Folding Pattern Used for Validation

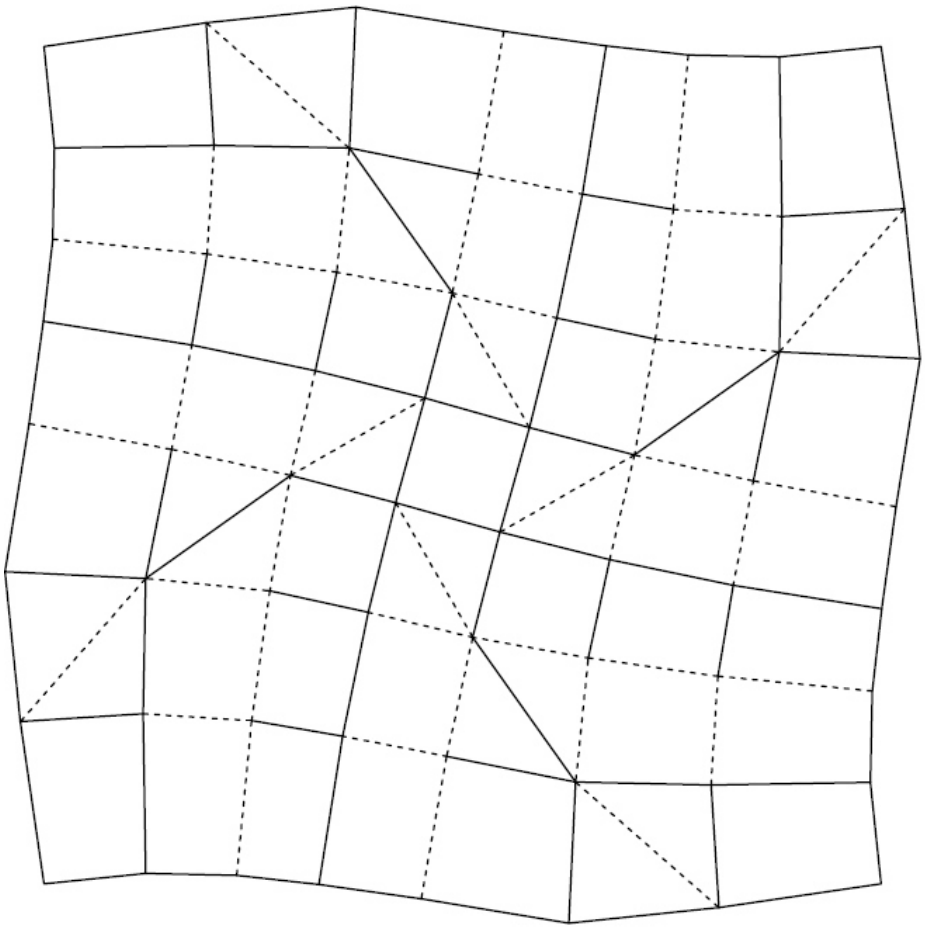

Appendix C - Input File of the Simulation

```
*Heading
** Job name: Deployment Model name: Model-1
** Generated by: Abaqus/CAE 6.12-3
*Preprint, echo=NO, model=NO, history=NO, contact=NO
**
** PARTS
**
*Part, name=Hub
*Node
      1,          -5.,       -4.375,           0.
      2,       -4.375,       -4.375,           0.
      3,       -4.375,        -3.75,           0.

... ... ...

      439,        0.625,        1.875,           0.
      440,       4.6875,       -0.625,           0.
      441,       -0.625,       -3.125,           0.
*Element, type=S4
1,   1, 122, 342, 125
2, 122,   2, 123, 342
3, 125, 342, 124,   4

... ... ...

398, 137,  12, 339, 441
399, 329, 441, 216,  59
400, 441, 339,  60, 216
*Nset, nset="Edge 1"
  85,  86, 106, 107, 108, 109, 110, 111, 112, 113, 114, 256, 289,
291, 293, 295
 297, 299, 301, 303, 305
*Elset, elset="Edge 1"
 199, 200, 247, 248, 251, 252, 255, 256, 259, 260, 263, 264, 267,
268, 271, 272
 275, 276, 279, 280

... ... ...

*Elset, elset="_Top Surface_SPOS", internal, generate
   1,  400,    1
*Surface, type=ELEMENT, name="Top Surface"
"_Top Surface_SPOS", SPOS
*Elset, elset="_Bottom Surface_SNEG", internal, generate
   1,  400,    1
*Surface, type=ELEMENT, name="Bottom Surface"
"_Bottom Surface_SNEG", SNEG
```

```
** Section: Shell
*Shell Section, elset=Shell, material="Kapton Polymide Film",
controls=EC-1, section integration=GAUSS
0.025, 2
*End Part
**

... ... ...

**
**
** ASSEMBLY
**
*Assembly, name=Assembly
**
*Instance, name=Hub-1, part=Hub
*End Instance
**
*Instance, name="Triangle 1-1", part="Triangle 1"
          0., 4.98750003909446, 4.99998437507332
          0., 4.98750003909446, 4.99998437507332,          -1.,
4.98750003909446, 4.99998437507332, 89.8567615193099
*End Instance
**
*Instance, name="Rectangle 1-1", part="Quadrilateral 1"
-4.9626918375454, 9.9749279389271, 5.0248084643593
-4.9626918375454, 9.9749279389271, 5.0248084643593, -
5.54052061105731, 9.39709613077589, 5.60119750842861,
119.58814750458
*End Instance
**

... ... ...

*Element, type=CONN3D2
1, Hub-1.85, "Triangle 1-1".3
*Connector Section, elset=Wire-1-Set-1, behavior="Crease - Regular"
Cardan,
"Datum csys-3",
*Element, type=CONN3D2
2, Hub-1.106, "Triangle 1-1".2
*Connector Section, elset=Wire-2-Set-1, behavior="Crease - Regular"
Cardan,
"Datum csys-4",

... ... ...

*Element, type=CONN3D2
768, "Rectangle 3-4".77, "Rectangle 4-4".33
```

```
*Connector Section, elset=Wire-768-Set-1, behavior="Crease -
Regular"
Cardan,
"Datum csys-770",
*Nset, nset=Wire-1-Set-1, instance=Hub-1
 85,
*Nset, nset=Wire-1-Set-1, instance="Triangle 1-1"
 3,
*Elset, elset=Wire-1-Set-1
 1,
*Nset, nset=Wire-2-Set-1, instance=Hub-1
 106,
*Nset, nset=Wire-2-Set-1, instance="Triangle 1-1"
 2,
*Elset, elset=Wire-2-Set-1
 2,

... ... ...

*Nset, nset=Wire-768-Set-1, instance="Rectangle 3-4"
 77,
*Nset, nset=Wire-768-Set-1, instance="Rectangle 4-4"
 33,
*Elset, elset=Wire-768-Set-1
 768,
*Surface, type=NODE, name="Hub-1_Edge 1_CNS_", internal
Hub-1."Edge 1", 1.
*Surface, type=NODE, name="Triangle 1-1_Edge 2_CNS_", internal
"Triangle 1-1"."Edge 2", 1.
*Surface, type=NODE, name="Hub-1_Edge 2_CNS_", internal
Hub-1."Edge 2", 1.

... ... ...

*Surface, type=NODE, name="Rectangle 2-4_Edge 2_CNS_", internal
"Rectangle 2-4"."Edge 2", 1.
*Nset, nset="_T-Datum csys-2", internal
"Rectangle 4-1"."Pull Corner",
"Rectangle 4-2"."Pull Corner",
"Rectangle 4-3"."Pull Corner",
"Rectangle 4-4"."Pull Corner",
*Transform, nset="_T-Datum csys-2", type=C
          0.,           0.,           0.,           0.,
0.,           1.
*Orientation, name="Datum csys-3"
          1.,           0.,           0.,           0.,
1.,           0.
1, 0.
*Orientation, name="Datum csys-4"
```

```
... ... ...

1, 0.
*Orientation, name="Datum csys-770"
0.00887428028066012, 0.999925628790737, -0.00836564623619542, -
0.727597999707696, 0.0121957733436172, 0.685895337448733
1, 0.
** Constraint: Tie - Hub T 1-1
*Tie, name="Tie - Hub T 1-1", adjust=yes, no rotation, type=SURFACE
TO SURFACE, no thickness
"Triangle 1-1_Edge 2_CNS_", "Hub-1_Edge 1_CNS_"
** Constraint: Tie - Hub T 1-2
*Tie, name="Tie - Hub T 1-2", adjust=yes, no rotation, type=SURFACE
TO SURFACE, no thickness
"Triangle 1-2_Edge 2_CNS_", "Hub-1_Edge 2_CNS_"
** Constraint: Tie - Hub T 1-3

... ... ...

*Tie, name="Tie - T 4-4 Q 2-4", adjust=yes, no rotation,
type=SURFACE TO SURFACE, no thickness
"Rectangle 2-4_Edge 2_CNS_", "Triangle 4-4_Edge 1_CNS_"
*End Assembly
*Connector Behavior, name="Crease - Regular"
*Connector Elasticity, component=4
 0.226,
*Connector Behavior, name="Crease - Diagonal"
*Connector Elasticity, component=4
 0.32,
**
** ELEMENT CONTROLS
**
*Section Controls, name=EC-1, second order accuracy=YES
1., 1., 1.
*Amplitude, name=SmoothStep, time=TOTAL TIME, definition=SMOOTH
STEP
             0.,              0.,              2.,              1.
**
** MATERIALS
**
*Material, name="Kapton Polymide Film"
*Density
 1.42e-06,
*Elastic
 2.5e+06, 0.34
**
** INTERACTION PROPERTIES
**
```

```
*Surface Interaction, name=Frictionless
*Friction
0.,
*Surface Behavior, pressure-overclosure=HARD
**
** BOUNDARY CONDITIONS
**
** Name: Pull Square 1 Type: Displacement/Rotation
*Boundary
"Rectangle 4-1"."Pull Corner", 1, 1
"Rectangle 4-1"."Pull Corner", 2, 2
** Name: Pull Square 2 Type: Displacement/Rotation
*Boundary
"Rectangle 4-2"."Pull Corner", 1, 1
"Rectangle 4-2"."Pull Corner", 2, 2
** Name: Pull Square 3 Type: Displacement/Rotation
*Boundary
"Rectangle 4-3"."Pull Corner", 1, 1
"Rectangle 4-3"."Pull Corner", 2, 2
** Name: Pull Square 4 Type: Displacement/Rotation
*Boundary
"Rectangle 4-4"."Pull Corner", 1, 1
"Rectangle 4-4"."Pull Corner", 2, 2
** ----------------------------------------------------------------
**
** STEP: Deployment
**
*Step, name=Deployment
*Dynamic, Explicit
, 2.1
*Bulk Viscosity
0.06, 1.2
** Mass Scaling: Semi-Automatic
**               Whole Model
*Fixed Mass Scaling, dt=1e-06, type=below min
**
** BOUNDARY CONDITIONS
**
** Name: Pull Square 1 Type: Displacement/Rotation
*Boundary, amplitude=SmoothStep
"Rectangle 4-1"."Pull Corner", 1, 1, 28.5
"Rectangle 4-1"."Pull Corner", 2, 2
** Name: Pull Square 2 Type: Displacement/Rotation
*Boundary, amplitude=SmoothStep
"Rectangle 4-2"."Pull Corner", 1, 1, 28.5
"Rectangle 4-2"."Pull Corner", 2, 2
** Name: Pull Square 3 Type: Displacement/Rotation
*Boundary, amplitude=SmoothStep
"Rectangle 4-3"."Pull Corner", 1, 1, 28.5
```

```
"Rectangle 4-3"."Pull Corner", 2, 2
** Name: Pull Square 4 Type: Displacement/Rotation
*Boundary, amplitude=SmoothStep
"Rectangle 4-4"."Pull Corner", 1, 1, 28.5
"Rectangle 4-4"."Pull Corner", 2, 2
**
** INTERACTIONS
**
** Interaction: General Contact
*Contact, op=NEW
*Contact Inclusions, ALL EXTERIOR
*Contact Property Assignment
 ,  , Frictionless
**
** OUTPUT REQUESTS
**
*Restart, write, number interval=1, time marks=NO
**
** FIELD OUTPUT: F-Output-1
**
*Output, field, variable=PRESELECT, time interval=0.01, time
marks=YES
**
** HISTORY OUTPUT: H-Output-1
**
*Output, history, time interval=0.001
*Energy Output
ALLAE, ALLIE, ALLKE, ALLSE, ALLVD, ALLWK, ETOTAL
**
** HISTORY OUTPUT: H-Output-2
**
*Node Output, nset="Rectangle 4-1"."Pull Corner"
RF1, RF2, RF3, U1, U2, U3
**

... ... ...

**
** HISTORY OUTPUT: H-Output-5
**
*Node Output, nset="Rectangle 4-4"."Pull Corner"
RF1, RF2, RF3, U1, U2, U3
*End Step
```